Voltage Imaging with Engineered Proton-Pumping Rhodopsins
Insights from the Proton Transfer Pathway

Meng, Xin; Ganapathy, Srividya; van Roemburg, Lars; Post, Marco; Brinks, Daan

DOI
10.1021/acsphyschemau.3c00003

Publication date
2023

Document Version
Final published version

Published in
ACS Physical Chemistry Au

ACS PHYSICAL CHEMISTRY Au
AN OPEN ACCESS JOURNAL OF THE AMERICAN CHEMICAL SOCIETY

pubs.acs.org/physchemau

Review

Voltage Imaging with Engineered Proton-Pumping Rhodopsins: Insights from the Proton Transfer Pathway

Xin Meng,[‡] Srividya Ganapathy,[*,‡] Lars van Roemburg, Marco Post, and Daan Brinks[*]

Cite This: https://doi.org/10.1021/acsphyschemau.3c00003

Read Online

ACCESS | Metrics & More | Article Recommendations

ABSTRACT: Voltage imaging using genetically encoded voltage indicators (GEVIs) has taken the field of neuroscience by storm in the past decade. Its ability to create subcellular and network level readouts of electrical dynamics depends critically on the kinetics of the response to voltage of the indicator used. Engineered microbial rhodopsins form a GEVI subclass known for their high voltage sensitivity and fast response kinetics. Here we review the essential aspects of microbial rhodopsin photocycles that are critical to understanding the mechanisms of voltage sensitivity in these proteins and link them to insights from efforts to create faster, brighter and more sensitive microbial rhodopsin-based GEVIs.

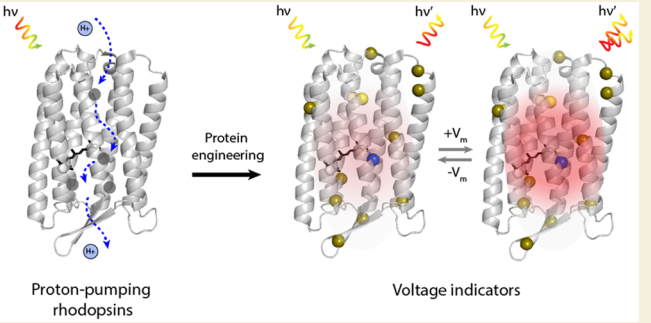

KEYWORDS: *microbial rhodopsins, genetically encoded voltage indicators, protein engineering, proton transfer pathway, biosensors, fluorescence microscopy, neuroscience, photophysics*

INTRODUCTION

Many organisms have developed photoreceptor proteins to help them adapt to the environment. These light-sensing proteins utilize different chromophores (including retinal, bilin and flavin) to transduce incoming photons into mechanical energy.[1,2] Rhodopsins are one such superfamily of retinal binding proteins, which are ubiquitous to all domains of life.[3] These proteins covalently bind a molecule of retinal, which is an aldehyde of vitamin-A derived from β-carotene.[3,4] The retinal chromophore absorbs a photon and undergoes isomerization in the protein environment.[4] This primary phototransduction event triggers distinct protein conformational changes leading to diverse functions ranging from ion transport to signal transduction.

Rhodopsins are divided into two distinct families based on phylogeny: type-1 (microbial rhodopsins) and type-2 (animal rhodopsins).[4,5] Type-1 or microbial rhodopsins use all-*trans* retinal as a chromophore to drive ion translocation or photosensory functions in several microbial species spanning Eukaryotes, Bacteria, and Archaea. Type-2 or animal rhodopsins form a specialized class of G-protein coupled receptors using 11-*cis* retinal as a chromophore and are responsible for visual and nonvisual phototransduction in vertebrates and invertebrates. Despite having almost no sequence homology, both animal and microbial rhodopsins share the same overall protein architecture of seven transmembrane α-helices (called the "opsin") which binds retinal.[3,4] The emergence of myriad functions and an expansive phylogeny from this common and relatively simple protein scaffold is nothing short of a spectacular feat of evolution. This is particularly stark for microbial rhodopsins, whose functions range from light-driven ion pumps or channels, phototaxis receptors to photoactivatable enzymes in several terrestrial and aquatic ecosystems. They play a key role in the survival and adaptation of their host microbes and can even exhibit spectral tuning to light availability in local microenvironments.[6] This supports the notion that microbial rhodopsins are essential to maintaining phototrophic energy balance in several biomes.[7] Recent advances in metagenomics have led to an explosion of discoveries of microbial rhodopsins in previously unexplored ecological niches. Their phylogenetic tree is continuously being expanded, with novel members with unknown functions being reported with some regularity.[8]

The incredible versatility of microbial rhodopsins have made them a tantalizing bioengineering platform. One of the greatest scientific revolutions of the last 20 years is the birth of Optogenetics.[9] A microbial rhodopsin termed channelrhodopsin, a cation channel responsible for phototaxis of green algae, was successfully applied as a light-gated actuator upon transgenic expression in mammalian neurons in 2005.[10] From this point onward, the application of microbial

Received: February 20, 2023
Revised: April 13, 2023
Accepted: April 13, 2023

rhodopsins has revolutionized neuroscience and influenced how we perturb, visualize, engineer, experiment on and think about the brain. Besides being used as actuators, proton-pumping microbial rhodopsins were engineered to report changes in membrane potential through their voltage modulated fluorescence.[11] This led to major advances in voltage imaging: visualizing cellular electrical dynamics in 3D and 4D fluorescence movies. The ability to directly transduce electrical dynamics into fluorescence sets genetically encoded voltage indicators (GEVIs) apart from genetically encoded calcium indicators (GECIs), which indirectly monitor neuron activity only through calcium influx.[12,13] Within the broader palette of GEVIs, different protein configurations have been used to convert changes in voltage into changes in fluorescence. These include voltage and pH sensitive ion channels or pumps containing a native chromophore, or voltage-sensing domains (VSDs) from voltage gated ion channels fused to fluorescent proteins (FPs). Despite their generally low fluorescence quantum yield, GEVIs based on proton-pumping microbial rhodopsins show faster response kinetics and the highest sensitivity to voltage changes, offsetting the higher brightness of VSD-FP sensors.[14−19] Efforts to create the next generation of GEVIs with improved brightness, faster kinetics, and higher voltage sensitivity have spawned a vibrant community of molecular biologists, protein engineers, physicists and neuroscientists working on engineering microbial rhodopsins.

The native function of microbial rhodopsins is typically described in terms of a photocycle: absorption of a photon starts a process converting the absorbed energy into a sequence of mechanical actions, typically isomerization of the retinal chromophore and subsequent conformational changes of the embedding protein, which for instance leads to transport of an ion through the protein. Each of these changes can be described as a transition out of and into an intermediate state of the protein: the structural features of each intermediate state are intimately linked to the lifetime of the state, its spectral properties (absorption spectrum, fluorescence and quantum yield) and the kind of perturbations it is sensitive to (for instance, application of voltage across the protein), which can lead to modification of the photocycle. Linking the mechanics and electromagnetic properties of the intermediate states is therefore necessary to understand the intrinsic ion translocation mechanism, the origin of the voltage sensitive fluorescence and the influence of protein and electrostatic modifications on both properties in microbial rhodopsins. This knowledge in turn informs our ability to improve the properties of microbial rhodopsin-based GEVIs. The first mutations in very early rhodopsin based GEVIs, namely the bacterial Proteorhodopsin and the archaeal Archaerhodopsin3, were meant to break the proton transfer pathway;[11] subsequent mutations were added to improve kinetics and state transitions toward more fluorescent states. The ion translocation mechanism (with proton transfer in Bacteriorhodopsin as an example), its impact on fluorescence, how it can be engineered and how it influences GEVI voltage sensitivity will be reviewed here.

PROTON TRANSFER IN BACTERIORHODOPSIN

For a detailed discussion of the mechanism of proton transport in microbial rhodopsins, we use the well-characterized bacteriorhodopsin (BR) as a model system. BR was discovered in the purple membrane of the halophilic archaea *Halobacterium salinarum* in 1970 and has since been extensively characterized, making it the best understood of all microbial rhodopsins.[3] All-*trans* retinal is covalently bound to a lysine residue (Lys 216 in BR) on the helix G through a Schiff base linkage, and this retinylidene Schiff base (RSB) is normally protonated (RSBH+).[3]

In the dark, the all-*trans* RSBH+ usually exists in an equilibrium with the 13-*cis* isomer (50:50 for BR), where steady-state illumination leads to a uniform all-*trans* population.[5,20] In the ground state, BR displays a maximum absorbance (λ_{max}) of ∼570 nm. After absorbing a photon, the RSBH+ enters the Franck−Condon S_1 state (H), from which several pathways are open to it: another absorption event can excite it into the Franck−Condon S_n state;[21,22] it can decay into the excited state intermediate I_{460} and from there decay back to the ground S_0 state through spontaneous emission (see next section) and nonradiative relaxation without further reaction; or it can enter the a reactive state from I_{460} characterized by photoisomerization at the C13═C14 double bond.[23,24] A general potential energy diagram of these reactions is shown in Figure 1. The all-*trans* → 13-*cis*

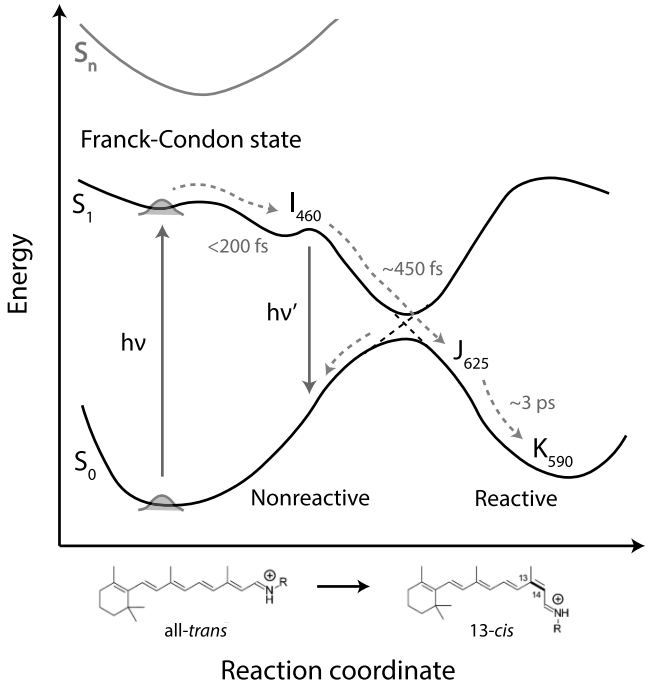

Figure 1. Potential energy diagram of the isomerization reaction of retinal in BR. Light absorption brings retinal into the Franck−Condon state from the ground state S_0. From the excited state S_1, the higher excited state S_n can be reached through a multiphoton process. After several hundred femtoseconds, a fraction of the molecules will decay back to the ground state through nonreactive fluorescence emission; the others will go through the photocycle resulting in translocation of a proton.

isomerization triggers a photochemical cycle containing a sequence of intermediate states, ultimately resulting in proton transfer[25−28] (Figure 2). These photointermediates can be distinguished and characterized by time-resolved spectroscopic and structure-based crystallographic methods.[27−32]

The transitions involved in photoisomerization (I → J → K) occur in the sub-ps to ps regime, and have been mapped using ultrafast spectroscopy and more recently in detail by time-

https://doi.org/10.1021/acsphyschemau.3c00003
ACS Phys. Chem Au XXXX, XXX, XXX−XXX

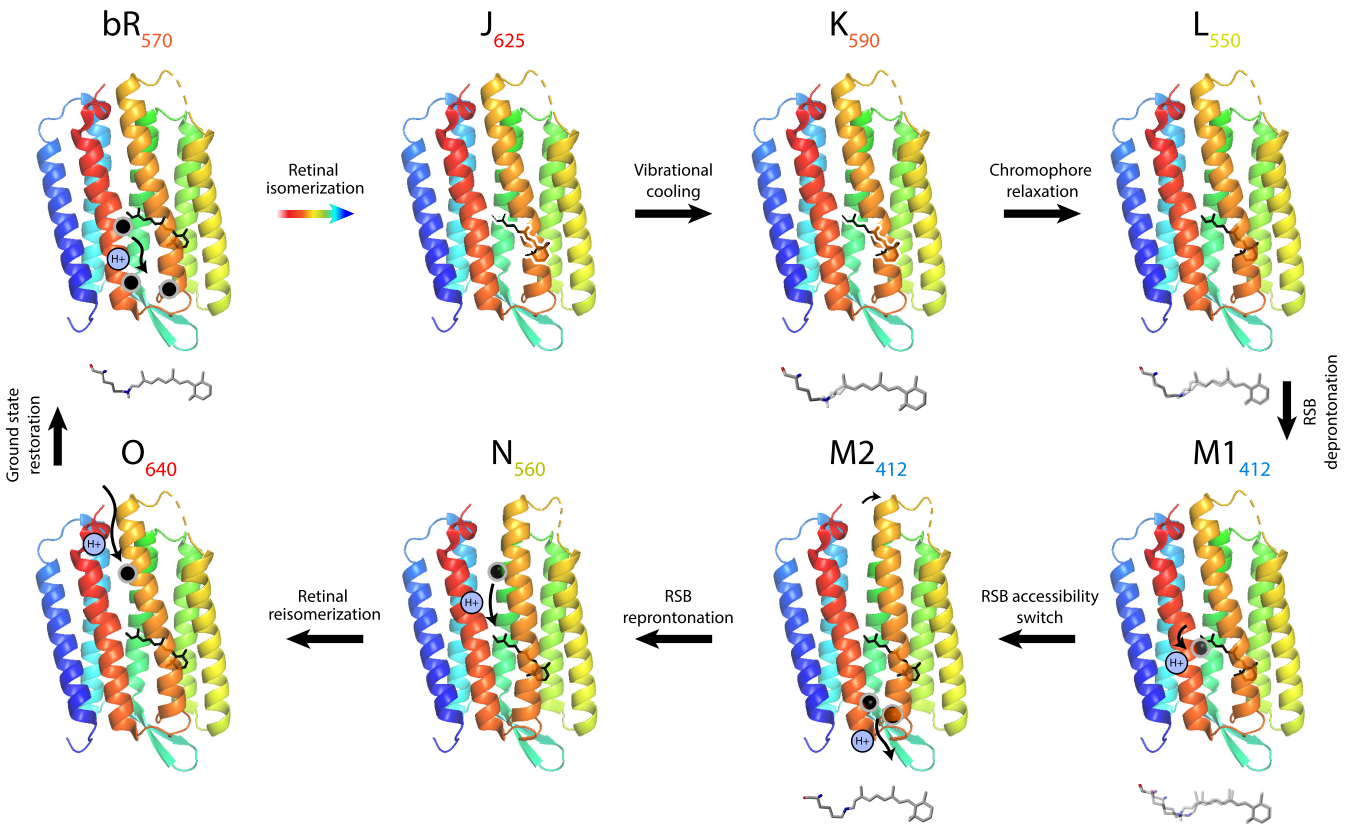

Figure 2. Illustration of the bacteriorhodopsin photocycle (PDB ID: 1C3W). L to M_1: proton transfer from RSBH+ to Asp85; M_1 to M_2: proton release from the proton release complex involving Glu194 and Glu204; M_2 to N: reprotonation of RSB from Asp96; N to O: reprotonation of Asp96 from the cytoplastic medium; O to bR: proton transfer from Asp85 to the proton release group. The maximum absorbance wavelength of each intermediate is labeled in number. The key residues involved in the transition are marked in black. Retinal structures indicate changes in geometry during the photocycle.[58]

resolved serial femtosecond crystallography.[33,34] Relaxation of the Franck−Condon to the reactive S_1 state occurs within 100−200 fs (reported values vary depending on measurements performed and their conditions), forming the blue-shifted electronically excited I_{460} intermediate, where the retinal is still all-*trans*.[35−39] This state decays via the conical intersection and forms the vibrationally hot J intermediate in 450 fs, resulting in the all-*trans* to 13-*cis* isomerization[40−42] (Figure 1). The J state is characterized by a twisted 13-*cis* RSBH+ geometry with a λ_{max} of 625 nm.[35,43] The transition to the K intermediate occurs in 3 ps along with a spectral shift from 625 to 590 nm[44−46] due to vibrational cooling and conformational relaxation of the chromophore[47,48] (Figure 2). The Raman spectrum of the K state has a strong 13-*cis* chromophore fingerprint, indicating that the all-trans to 13-*cis* isomerization is complete.[48,49] Compared to the highly twisted J intermediate, the K intermediate is characterized by a more planar retinal chromophore.[48] After ∼70 ps, the protein−retinal complex undergoes further relaxation identified by Raman spectroscopy and renewed hydrogen out-of-plane (HOOP) intensity.[29,48] This state, termed the KL intermediate, leads to a stronger hydrogen bond association between the RSBH+ and the proton acceptor Asp85.[29]

The L intermediate forms within ∼1.5 μs and is spectrally close to the K intermediate.[50] FTIR spectroscopy indicates that the KL to L transition involves structural relaxation of the Schiff base and the β-ionone region of retinal with different kinetics.[29,50] During the transition from K → KL → L, the distorted chromophore relaxes and the energy this releases is utilized for rearrangement of the protein environment.[50−52] These perturbations help overturn the proton affinity between RSBH+ (high) and Asp85 (low), facilitating the proton transfer to Asp85 during the subsequent transition from L → M intermediate.[3,29,53,54] Rearrangement of the hydrogen bonding network involving the three water molecules in the cavity facilitates deprotonation of the RSBH+.[55−57] Water402 in particular plays an important role here, since it interacts directly with RSBH+, and the counterions Asp85 and Asp212[56,57] (Figure 3). In the L intermediate, the hydrogen bonds between Water402 and Asp85, and between Water402 and the N−H group from RSBH+ are strengtehend.[28,56] This lowers the pK_a of RSBH+, destabilizes the RSB proton, and maintains the negative charge at Asp85, which facilitates the deprotonation process.[50,56,57]

This transfer happens in around 10−40 μs as confirmed by FTIR.[28,59] Water402 potentially switches its hydrogen bond from Asp85 to Asp212 during the L to M transition and improves the deprotonation efficiency.[57]

The proton transition to Asp85 marks the formation of the M intermediate, which is characterized by the deprotonated chromophore with a blue-shifted λ_{max} at ∼400 nm[60] (Figure 2). Upon decay of the M intermediate, the RSB is reprotonated by the proton donor Asp96 situated 10 Å away on the cytoplasmic side.[3,28,29] The defining feature of the M state is a switch in accessibility of the RSB from the extracellular to the cytoplasmic part of the protein, breaking

https://doi.org/10.1021/acsphyschemau.3c00003
ACS Phys. Chem Au XXXX, XXX, XXX−XXX

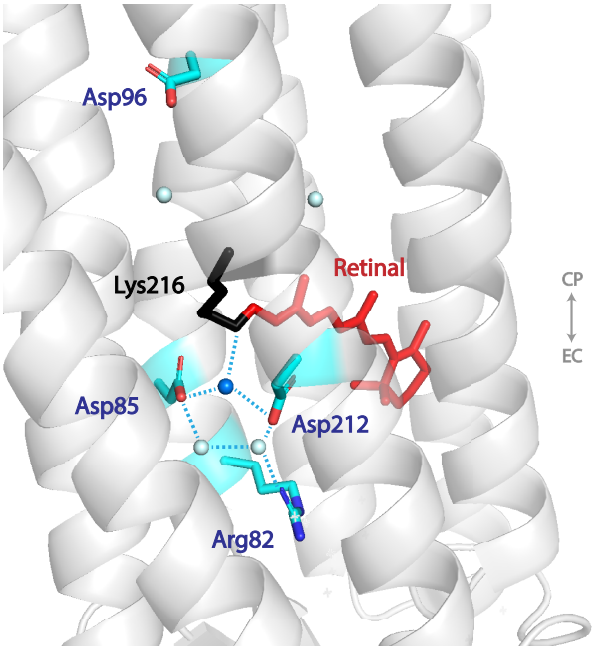

Figure 3. Structure of the RSB region in BR (PDB ID: 1C3W). The retinal chromophore is linked to the helix through Lys216. There are three water molecules (water402 in blue, water401, and water406) found in between the RSB and the proton acceptor Asp85. Potential hydrogen bonds are shown in dashed lines. Cytoplasmic side (CP) and extracellular side (EC) directions are marked in light gray in Figures 3−6.

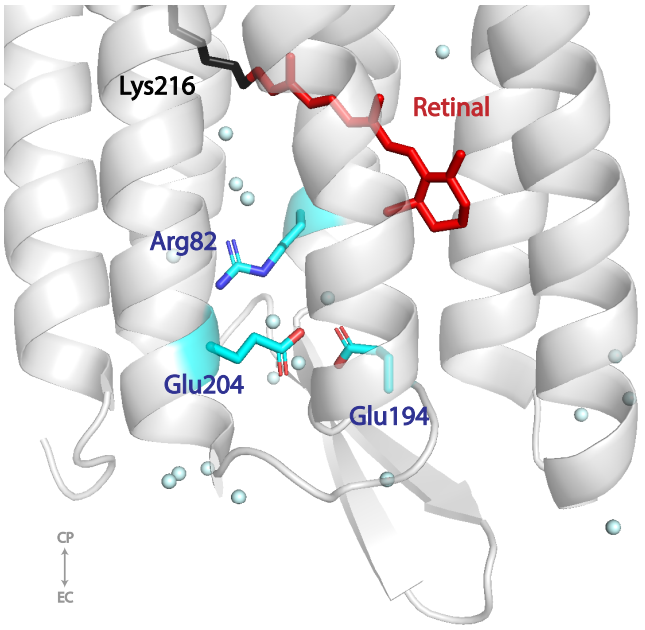

Figure 4. Structure of the proton release region in BR. Multiple side chains and water molecules are involved in the proton release process. The key residues, Glu194, Glu204, and Arg82, are illustrated here.

extracellular access and ensuring vectorial proton pumping. This switch is facilitated by a structural change in the RSB and movement of the protein helices F and G.[58,61−65] Proton transfer from the RSB to Asp85 breaks its electrostatic interactions with the extracellular facing residues leading to a distortion in the chromophore. From X-ray crystallography, it was shown that deprotonation leads to an unbending of retinal due to a decrease in its intrinsic curvature.[63,66] A complementary view has been provided by magnetic resonance studies, where breaking the "electrostatic yoke" holding the RSB, Asp85 and the surrounding hydrogen-bonded network leads to a release in torsion of the RSB.[65,66] Concomitantly, an outward tilt of the helix F and movement in the cytoplasmic end of helix G together shape a cytoplasmically open state that facilitates efficient reprotonation of the SB.[65,67−71] It is likely that these changes occur in a sequential way, i.e. that the distortions in the RSB trigger its rearrangement toward the cytoplasm.[63,72] This accessibility switch was discovered in the late 90s and has since been incorporated in the photocycle as the transition event from the M_1 to the M_2 intermediate[64] (Figure 2). The M_2 to M_1 back reaction rate was found to increase with increasing proton concentration.[64] The M_2 intermediate accumulates at higher hydration levels than M_1 and the associated conformational change is reversed at the end of the photocycle.[72]

A putative proton release group is responsible for releasing the proton into the extracellular medium during the M state, as Asp85 stays protonated until the end of the photocycle.[3,28,64,73] The exact identity of this proton release group is unknown, though it likely involves a water cluster containing one proton, five water molecules and several residues including Glu204, Glu194 and Arg82[28,73,74] (Figure 4). The protonation status of this group was found to be coupled to that of the counterion Asp85.[75−77] When the counterion is protonated, the pK_a of the proton release group is low (∼5), resembling dissociation; when the counterion is anionic, the pK_a of the release group is high (∼9.2), indicating that Asp85 protonation leads to extracellular proton release.[28,75,76] During the transition from $M_1 \rightarrow M_2$, protonation of Asp85 displaces the Arg82 side-chain toward Glu194 and Glu204, which stabilize a fluctuating excess proton in the release site.[78,79] The approaching Arg82 breaks this balance, thereby releasing the proton extracellularly.[74] This early extracellular proton release is a key event in proton transfer, as the coupled rise in pK_a of Asp85 prevents back-transfer to the RSB, ensuring the $M_1 \rightarrow M_2$ directionality.[73]

The formation of the subsequent N intermediate (Figure 2) occurs in around ∼5 ms,[3,70] and is accompanied by proton transfer from the donor Asp96 to the RSB. The structural changes involved in the transition from $M_1 \rightarrow M_2 \rightarrow N$ (e.g., the outward tilt of helix F) allow water to enter the RSB vicinity forming the cytoplasmic proton transfer water cluster.[28,30,80,81] The crystal structure of the accumulated N state displayed a continuous chain of single-file hydrogen-bonded water molecules connecting Asp96 and RSB, serving as the proton conducting pathway.[80,82,83] The actual time required to complete this movement (ms) is 6 orders of magnitude longer than in theory (ns), because of the slow kinetics of prerequisite conformational changes and deprotonation of Asp96.[28,82,84,85]

The reprotonation of Asp96 is accompanied by thermal reisomerization of retinal back to all-*trans* upon decay of the N intermediate and start of the O intermediate.[28,86] Protons are taken up from the cytoplasmic surface to protonate Asp96 during this transition.[25] The reisomerization of retinal and reprotonation of Asp96 are thought to be coupled by turning of the RSB N−H bond, which collapses the water chain connecting RSB and Asp96 leading to an increased proton affinity of Asp96.[28,87] The exact mechanism of Asp96 reprotonation is unknown, though it is hypothesized that a group of cytoplasmic residues (Asp36, Asp38, Asp102, Asp104,

https://doi.org/10.1021/acsphyschemau.3c00003
ACS Phys. Chem Au XXXX, XXX, XXX−XXX

and Glu166) attract protons though the narrow tunnel toward Asp96, which becomes wider during the movement of helix F (Figure 5).[88−91]

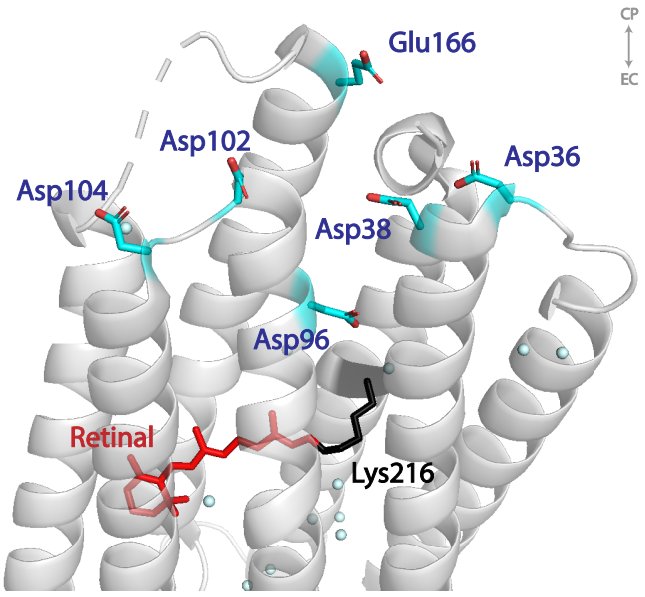

Figure 5. Structure of the proton uptake region in BR. Multiple residues, including Asp36, Asp38, Asp102, Asp104, and Glu166, are likely to be involved in the reprotonation process of the proton donor Asp96 during the photocycle.

Resonance Raman spectra of the O intermediate displays intense HOOP vibrations arising from distortions in the all-*trans* chromophore relative to its ground state[86] (Figure 2). The decay of O to ground state is the last step of the photocycle, which is characterized by reprotonation of the extracellular proton release group by Asp85.[28,92] Due to difficulty in resolving the structure and kinetics of the O intermediate, the mechanism of this long-distance transfer is still unknown.[93,94] The driving force is thought to be the difference in pK_a between Asp85 and the proton release group in the initial state.[28,95] It is suggested that Asp212 belongs to the Asp85-to-proton-release-group proton transfer pathway, and that Arg82, Glu194, and Glu204 participate in this transfer (Figure 4).[95−98] At the end of the O intermediate, the protein and the retinal are restored to the initial ground state completing the photocycle.

THE ORIGIN OF FLUORESCENCE

Microbial rhodopsins are weakly fluorescent in their dark state due to spontaneous emission of the RPSB. After photoexcitation and relaxation from the Franck−Condon state, the RPSB can enter the nonreactive S_1 state emitting a photon relaxing back to the ground S_0. The quantum yield (QY) of fluorescence is low (in the order of 10^{-4}−10^{-5} for BR) since the RPSB is optimized to favor the photochemical reaction cycle, thereby leading to a high QY of photoisomerization (0.64 for BR).[99−103] This is consistent with a short excited state lifetime of ∼0.5 ps.[40,45] Early experiments on BR showed near-infrared fluorescence extending from 600 to 900 nm with a maximum at ∼740 nm and strong pH dependence.[99] Its emission band was found to be composite with contributions from photointermediate fluorescent states, in addition to spontaneous emission (BR568). These were determined to be the O intermediate and another highly fluorescent intermediate termed "Q", which arise from sequential absorption of 2 or 3 photons. Both O and Q have distinct decay kinetics (9 and 62 ps respectively) and their relative contribution toward fluorescence was shown to be dependent on the excitation power and pH.[104,105]

The red-shifted O-intermediate is characterized by an *all-trans* chromophore and protonated counterion. Fluorescence from O was found to be pH dependent with the fluorescence lifetime and QY decreasing with an increase in pH.[104,106] On the other hand, the Q intermediate is formed upon photoexcitation of the nonfluorescent N-intermediate, which is stabilized under alkaline conditions.[104] The quantum yield of Q is ∼100 times more than BR568.[106] It has a red-shifted absorption like O and its fluorescence lifetime is relatively insensitive to pH.[106] In fact, pH shifts the equilibrium between the N (branching to Q) and the O states, and therefore the emerging fluorescence.[106] The isomerization state of Q is likely to be all-*trans* since it is formed by photoexcitation of the 13-*cis* N state.[105,107] The accumulation of prefluorescent N can also be influenced in the preceding transition from M to N, which are both still within the 13-*cis* manifold. Optoelectric studies in BR showed that the ratio of M1/M2 intermediates and M2 decay were also found to be influenced by the electrochemical gradient.[108,109] Here, membrane potential is likely to impact the reprotonation of the RSB by D96, as the D96N mutant shows a slowing down of M decay.[84] Interestingly, in BR(D96N) illumination with blue/violet light leads to isomerization from the 13-*cis* M to an all-*trans* O-like state short circuiting the photocyle.[110,111] This type of optical switching between photostable all-*trans* and 13-*cis* intermediates has been reported in several other rhodopsins and is discussed in further detail in the next section with respect to voltage-sensitive fluorescence.[112−114]

The above studies in BR indicate that higher fluorescence is a property of the RPSB with a protonated counterion. This is supported by the longer excited state lifetimes of the BR upon acidification or neutralization of the counterion in the mutant D85N.[115,116] Recently, a highly fluorescent rhodopsin termed neorhodopsin (NeoR) was identified with a long excited state lifetime resulting in higher fluorescence QY.[114] NeoR has three Asp/Glu residues, neutralization of which leads to a sequential increase in QY and red-shifted absorbance band. Extrusion of water molecules from the active site is likely to contribute toward this process. NeoR was also found to cycle between a blue-shifted M-like state and a red-shifted state with a deprotonated chromophore similar to BR.[114]

The photointermediate fluorescence of BR was recapitulated in several studies done on variants of archaerhodopsin-3 (Arch3) from *Halorubrum sodomense*[18] which is widely used as a GEVI. The studies on highly fluorescent Arch3 variants indicate that the protein modifications may favor an all-*trans* O-like ground state (which is distinct from the ground state generated during protein biosynthesis) with a protonated RSB and a neutral Schiff base counterion. These studies are further explored in the next section.

THE ORIGIN OF VOLTAGE SENSITIVITY IN Arch3-BASED GEVIs

Investigations of the mechanism of Arch3 voltage sensitivity were carried out shortly after its application as GEVI.[117] Arch3 fluorescence was also thought to arise from a photointermediate, since the high illumination intensities typically

https://doi.org/10.1021/acsphyschemau.3c00003
ACS Phys. Chem Au XXXX, XXX, XXX−XXX

used to image Arch3 fluorescence should deplete the ground state. Using pump−probe spectroscopy, Arch3 fluorescence was found to arise from a three-photon process (similar to BR): the first photon initializes the photocycle, the second blue-shifted photon is absorbed by the N state branching the photocycle to Q and the third photon excites fluorescence from the Q state.[117] Through concurrent patch clamp and fluorescence experiments, it was confirmed that the voltage-sensitive fluorescence likely comes from a photointermediate with long lifetime.[117] It was hypothesized that the membrane potential tunes the equilibrium between the M and N state by affecting the RSB reprotonation efficiency from the proton donor D106[117] (Figure 6; equivalent to Asp96 in BR).

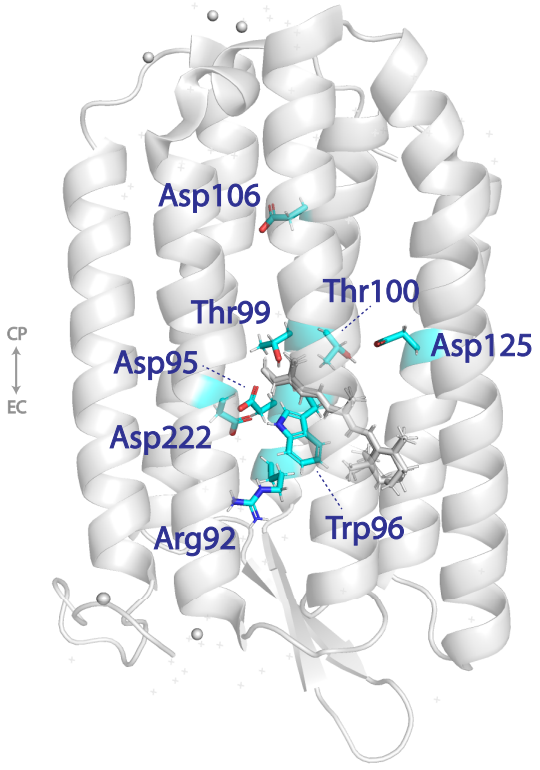

Figure 6. Key residues identified for the voltage sensing in Arch3 and Archon1 (PDB ID: 6GUZ).

Near-IR resonance Raman confocal microscopy studies on Arch3(D95N) (Figure 6; Asp95 is equivalent to the proton acceptor Asp85 in BR) demonstrated that an all-*trans* O-like intermediate predominates at neutral pH. At pH higher than 7, an N-like species is formed upon excitation of the O-like intermediate.[118] Arch3(D95N) accumulates 13-*cis* N-like species under red illumination, and voltage possibly influences the RSB protonation and therefore the equilibrium between M and N.[118] Combining ultraviolet−visible (UV−vis) absorption, fluorescence and FT-Raman spectroscopy, two Arch3 derivatives, QuasAr2 and NovArch, were found to be able to cycle between O-like and M-like states using 660 and 405 nm illumination.[119] The proton donor mutation D106H was thought to be responsible for the accumulation of the M-like state under red light, as lacking a proton donor to RSB inhibits the M → N transition.[119]

Recently a detailed characterization combining experiments and molecular dynamics (MD) simulations on Arch3 and its derivatives QuasAr1, QuasAr2, and Archon1 (described in further detail below) showed different mechanisms of generating voltage sensitive fluorescence.[120] Steady-state UV−vis and time-resolved pump−probe spectroscopy on QuasAr1 and QuasAr2 showed that they have orders of magnitude extended excited state lifetimes (4−40 ps) compared to Arch3, and that only a small fraction of the chromophores (4% for QuasAr2 and 1% for QuasAr1) undergo heterogeneous isomerization.[120] In another Arch3 derivative Archon1, the excited-state lifetime is even longer (around 70 ps) with 0.1% isomerization efficiency. These observations further strengthened the conclusion that neutralizing the counterion prolongs the excited-state lifetime and increases the fluorescence.[120] To further investigate the origin of voltage sensitivity, atomistic MD simulations were carried out based on a homology model of Arch3. From the simulations, application of voltage across Arch3 triggers reorientation of R92 (equivalent to R82 in BR), which in turn leads to a reorganization of the hydrogen bonded network.[120] Thus, at higher voltage water molecules were prohibited from entering the RSBH+ vicinity, and a new hydrogen bond involving Asp95 was established. Both the lack of water molecules near RSBH+ and formation of a separate hydrogen bond involving D95 disfavor the RSBH+ deprotonation.[120] In contrast, in Archon1 the crucial voltage induced reorientation was found to be the intracellular residue D125. Movement of the protein scaffold at positive voltage removes the D125-T100 hydrogen bond, and forms Q95-T99 and T100-W96 hydrogen bonds (Figure 6). This rearrangement creates a more rigid chromophore environment and strengthens the RSBH+D222 hydrogen bond. Although the exact mechanism of voltage sensitivity is still unclear, the studies in Arch3 indicate that the membrane potential tunes the equilibrium in protonation status of RSB and its counterion via reorganization of the hydrogen bonding network.[120]

ENGINEERING OPSIN-BASED GENETICALLY ENCODED VOLTAGE INDICATORS

In the past decade, microbial rhodopsin based GEVIs have evolved remarkably, in parallel with efforts to understand their mechanisms of voltage sensitivity. Both evolutionary approaches and targeted mutagenesis approaches have led to significant results, which we review in the next section.

The first microbial rhodopsin-based GEVI, termed PROPS, was based on the bacterial proteorhodopsin (GPR) as a starting scaffold. GPR was mutated at the counterion Asp97 for pH-modulated fluorescence, and the mutant revealed electrical spiking in *Escherichia coli*.[11,121] Despite the decent voltage sensitivity ($\Delta F/F$ = 150% per 100 mV) and speed, PROPS shows poor membrane expression in mammalian cells.[11,18] Further screening of microbial rhodopsins that localize well to the eukaryotic membrane led to the application of Arch3.[18] Arch3 was first introduced as an optical silencer allowing significant firing rate suppression within milliseconds.[122]

It was later discovered that Arch3 showed fast fluorescence changes modulated by membrane potential upon expression in HEK293 cells.[18] To eliminate the photocurrent measured under standard neural imaging illumination (10 pA, I = 1800 W/cm^2), the Arch3 counterion D95 was mutated to an uncharged Asn, analogous to studies on BR[18,123] (Figure 7). The resulting mutant, Arch3(D95N) has no photocurrent, shows lower RSB pK_a and displays 50% greater sensitivity ($\Delta F/F$ = 60% per 100 mV) at the cost of slower kinetics (41 ms).[18]

https://doi.org/10.1021/acsphyschemau.3c00003
ACS Phys. Chem Au XXXX, XXX, XXX−XXX

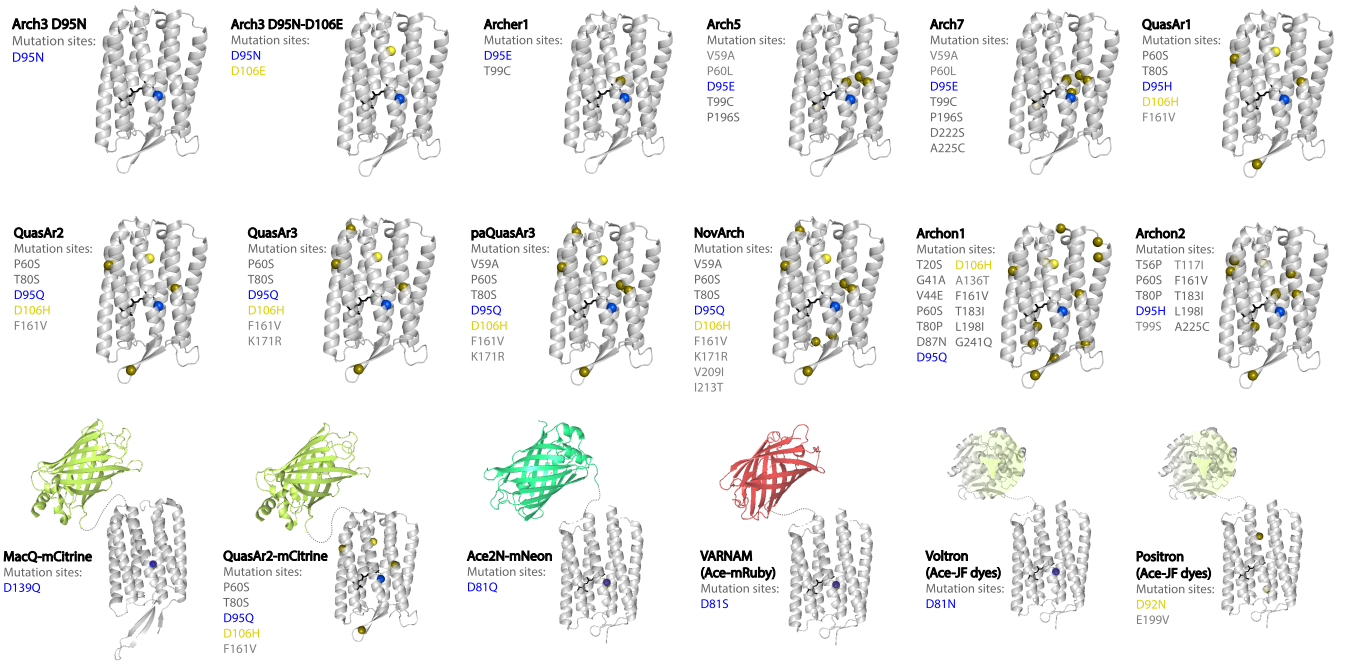

Figure 7. Illustration of mutation sites of rhodopsin-based GEVIs compared to the wild-types. Mutations at the counterion are highlighted in blue, and mutations at the proton donor are highlighted in light yellow. Mutations at the other sites are shown as dark yellow spheres in the structure illustration.

Through rational site-directed mutagenesis based on Arch3-(D95N), the double mutants Arch3(D95N/D106E) and Arch3(D95Q/D106E) were found to exhibit an improved response speed.[124] The extra mutation on the proton donor D106 was thought to alter the RSB protonation and deprotonation kinetics.[124]

A major drawback of the Arch3 sensors is their extremely low quantum yield. Although the red-shifted excitation wavelength is favorable for deep tissue imaging, it requires high illumination intensities which is not suitable for *in vivo* applications.[125] The main goal in the evolution of Arch3 was therefore improving its brightness. The red-shifted Arch3-(D95E/T99C) was used as a template for directed evolution.[126] As a powerful way to engineer protein properties, directed evolution uses random mutagenesis to generate a pool of mutant libraries, and iterative selection is applied to direct the library performance. Through evolutionary screens, three individual mutations (V59A, P60L, and P196S) were found to improve the brightness.[127] Combining with site-saturation mutagenesis, two mutants, termed Arch5 (V59A/P60L/D95E/T99C/P196S) and Arch7 (V59A/P60L/D95E/T99C/P196S/D222S/A225C) exhibit around 20-fold increase in brightness compared to Arch3[127] (Figure 7). This study demonstrated that mutations at other sites besides the counterion could influence the fluorescence quantum yield.[115,127] Arch3(D95E/T99C) and Arch3(D95E/T99C/A225M) were then characterized in primary neuronal cultures and applied to track sensory neurons in *Caenorhabditis elegans*, and named Archer1 and Archer2 respectively.[125] Both however still show a steady photocurrent of 10 pA under 880 mW/mm^2 illumination.[125]

The first Arch3-based GEVIs which found successful applications in neuroscience were engineered using Arch3-(D95N) as a template, where several rounds of directed evolution yielded two non-pumping variants. QuasAr1 (mutation sites compared to Arch3 P60S/T80S/D95H/D106H/F161V) and QuasAr2 (H95Q compared to QuasAr1; Figure 7) showed the best performance in terms of brightness, voltage sensitivity, and kinetics, respectively (15 times and 3.3 times brighter than Arch3, 32% and 90% $\Delta F/F$ per 100 mV, 0.053 and 1.2 ms response fast time constant).[128] The first five screening iterations resulted in four extra mutation sites (P60S, T80S, D95N, D106Y, and F161V), with T80 and F161 lying at the periphery of the protein.[128] This was followed by a full investigation focusing on the D95 and D106 to further tune the voltage sensitivity and kinetics, leading to the substitutions N95H and Y106H.[128] Combining QuasAr with a sensitive blue-shifted channelrhodopsin variant CheRiff, all-optical electrophysiology (combined optical stimulation and recording of electrophysiological signaling in neurons) was carried out *in vitro*.[128,129]

Following this, a high-throughput multidimensional directed evolution screen was carried out based on QuasAr2.[130] FACS sorting was performed first to eliminate nonfluorescent mutants, and a second stage microscopy-guided robotic cell picking was applied which evaluated cells in a multiple parameter space.[130] The final two chosen mutants, Archon1 (mutation sites compared to Arch3: T20S/G41A/V44E/P60S/T80P/D86N/D95Q/D106H/A136T/F161V/T183I/L197I/G241Q) and Archon2 (mutation sites compared to Arch3: T56P/P60S/T80P/D95H/T99S/T116I/F161V/T183I/L197I/A225C; Figure 7), exhibit 2.4 and 6.8 times increased brightness compared to QuasAr2, while retaining voltage sensitivity (81% and 20% $\Delta F/F$ per 100 mV).[130] In addition to the counterion and proton donor, the remaining mutation sites are spread over the whole protein structure. These constructs were used to detect subthreshold neural activity in acute mouse brain slices and in larval zebrafish *in vivo*.[130]

These sensors were further engineered to improve their *in vivo* signal-to-noise (SNR) for application in behaving mice.

https://doi.org/10.1021/acsphyschemau.3c00003
ACS Phys. Chem Au XXXX, XXX, XXX−XXX

QuasAr3 was developed through rational design and hierarchical screening to improve the membrane trafficking in neurons, which is a limiting factor for *in vivo* expression.[131] The construct combines a mutation in an intracellular loop (K171R), optimized fusion protein linker and soma-localized opsin expression. Further investigation on the effects of previously found mutation sites led to the discovery of paQuasAr3 (mutation sites compared to QuasAr2: K171R and V59A; Figure 7) which displays 2−3-fold brightness over QuasAr3 and two times the spike detection SNR under concomitant blue illumination.[131] A simultaneous dual-wavelength patterning microscope was developed to perform cell targeted illumination, which decreased background noise and increased the SNR by a factor of 3.5−11.[131] Populational neuron activities were monitored in different brain regions while the head-fixed mice were walking or anaesthetized, and electrical compartmentalization of the dendrites was observed.[131]

Continuing the directed evolution on paQuasAr3, a brightness-enhanced variant, NovArch (mutation sites compared to parent: V209I/I213T; Figure 7), was found.[132] Under blue illumination (12 W/cm^2), it shows a 4.8-fold fluorescence enhancement, and is around twice as bright as paQuasAr3.[132] More importantly, it is activatable under two-photon (2P) illumination, displaying a 2.7-fold fluorescence enhancement while maintaining the same voltage sensitivity ($\Delta F/F$ = 41% per 100 mV).[132] It was demonstrated in acute brain slices (40 to 70 μm deep) that NovArch exhibited a 3.5-fold enhanced spike amplitude and SNR of 96 under 2P enhancement.[132] *In vivo* experiments in behaving mice showed that the spike SNR increased from 4 to 6.8 with the addition of blue light.[132]

In the meantime, a soma localized version of Archon1, SomArchon, was developed which showed 2-fold greater sensitivity in neurons compared to Archon1 while maintaining comparable kinetics and SNR (about 7−16 per action potential).[133] It was applied to report neuron dynamics in behaving mice across different regions, and achieved simultaneous recording from 14 neurons in the hippocampus using a conventional microscope.[133] Later, SomArchon was paired with SomCheRiff to perform all-optical interrogation on synaptic inputs of L1 interneurons in awake mice.[134]

Despite all these engineering efforts, the quantum yield of microbial rhodopsin-based GEVIs is still 2 orders of magnitude lower than conventional fluorescent proteins.[135,136] As an alternative approach to cope with this drawback, microbial rhodopsins can be paired with fluorescent proteins having an emission spectrum that overlaps with the rhodopsin absorption spectrum, and form an eFRET (electrochromic Förster resonance energy transfer) indicator.[137] In this case, the rhodopsin serves as a voltage sensor and FRET acceptor: its membrane-potential-modulated absorption spectrum will affect the quenching of the FRET donor, resulting in a change in the brightness of the fluorescent protein.[138] The resulting GEVI retains part of the voltage sensitivity of the rhodopsin and exhibits the bright fluorescence and high quantum yield of the fluorescent protein.

A blue-shifted proton pump *Leptosphaeria maculans* (Mac) with a slow photocycle was first paired with mCitrine to form the eFRET sensor, MacQ-mCitrine.[139] Similar to Arch3, mutations were engineered at the counterion D139 (Figure 7) and proton donor D150, though the proton donor mutation introduced slow kinetics.[124,139] MacQ-mCitrine was applied to report spiking events from dendrites of Purkinje neurons in live mice (illumination intensity 10 mW/mm^2).[139] QuasAr2 was also used as a acceptor in several eFRET sensors.[140] The optimal length of the linker between the donor and acceptor was determined through screening of linker truncation libraries. Different fluorescent proteins were paired with QuasAr2, and mCitrine showed the largest sensitivity ($\Delta F/F$ = −13.1% per 100 mV).[140] The resulting GEVI (QuasAr2-mCitrine) was able to report spikes in cultured neurons with a SNR of 7−9 under low excitation power (30 mW/mm^2).[140] Both MacQ-mCitrine and QuasAr2-mCitrine show a millisecond range fast time constant (2.8 and 4.8 ms respectively).[139,140]

To further improve upon the kinetics of eFRET voltage sensors, a mutant of the fast rhodopsin derived from *Acetabularia acetabulum* (Ace, mutation at the counterion D81, Figure 7), was fused with a fluorescent protein, mNeonGreen, to generate the sensor Ace-mNeon.[141] In cultured neurons, Ace2N-mNeon shows a $\Delta F/F$ of 12% and sub-millisecond response (fast time constant = 0.37 ms, governs 58% of response).[141] The fast response time allows Ace-mNeon to detect spikes with high-accuracy with spike-timing errors of 0.24 ± 0.01 ms in mice and 0.19 ± 0.002 ms in flies.[141] Later, Ace2N was fused to the red fluorescent protein mScarlet, and the resulting sensor Ace-mScarlet displays comparable performance while avoiding potential crosstalk when used with blue-shifted Optogenetics actuators.[142]

In the search for better red-shifted eFRET sensors, Ace fused with the bright red fluorophore mRuby3 was subjected to high-throughput screening optimizing Ace mutations and the linker to improve the sensitivity.[143] The resulting construct, Ace-WR-mRuby3 N81S (VARNAM, Figure 7), showed comparable sensitivity to Ace-mNeon when imaged under 565 nm excitation.[143] All-optical electrophysiology experiments were carried out using CheRiff and VARNAM in acute slices. Under these imaging conditions, optical crosstalk of imaging VARNAM generated a constant photocurrent of around 35 pA from CheRiff-positive neurons, which was however reasoned to be negligible.[143] Proof-of-concept dual-color simultaneous imaging of Ace-mNeon and VARNAM expressed in different types of *Drosophila* neurons was performed under 488 and 565 nm illumination.[143]

As the quantum yield of the protein is a bottleneck in achieving populational neuron imaging, synthetic fluorescent dyes, which are significantly brighter, are also used as donors in eFRET designs.[144] In a FRET design that utilizes Ace2N as the voltage sensing domain, a dye-capturing protein domain, HaloTag, which irreversibly binds the Janelia Fluor (JF) dyes, is linked as a FRET donor.[145] The combined chemogenetic sensor (Voltron, Figure 7), is 3−4 fold brighter and is 8 times more photostable than Ace2N-mNeon. It shows a high sensitivity of −23%% $\Delta F/F$ per 100 mV.[145] Voltron could be used to monitor the activity of 449 neurons from 12 field of views at 400 Hz in living mice, under moderate illumination intensity (3 to 20 mW/mm^2).[145]

A disadvantage of eFRET GEVIs is that they show high fluorescence at cellular resting potentials and at neutral voltages, and that they generally show a negative response to voltage. Thus, the background fluorescence from non-membrane-trafficked GEVIs and nontarget cells can easily overwhelm the signal of active target cells, leading to low SNR, especially in tissue and *in vivo* recordings. A solution to this problem is to invert the polarity of the fluorescence response to voltage of the rhodopsin voltage sensing domain. A general

https://doi.org/10.1021/acsphyschemau.3c00003
ACS Phys. Chem Au XXXX, XXX, XXX−XXX

rational approach to flip the voltage sensitivity of rhodopsins was eventually presented based on findings in Ace.[146] Based on the transient inward photocurrent of the Ace(D81N), it was reasoned that the voltage sensitivity stems from the protonation equilibrium between RSB and the cytoplasmic proton transfer network.[146] Blocking the proton donor D92 was hypothesized to switch accessibility of RSB protonation to the extracellular side. This would result in an opposite protonation equilibrium reversing the polarity of the fluorescence response.[146] Experimentally, Voltron D92N indeed displays a positive voltage sensitivity, albeit with slower kinetics. The kinetics were improved by reverting to the negative counterion (N81D),[146] but a 40% loss in sensitivity was observed. Saturation mutagenesis was performed on E199 which possibly mediates the protonation equilibrium of the RSB.[146] The E199V mutant was found to have two times the sensitivity over Voltron N81D D92N, and was named Positron (Figure 7). Similar results were obtained upon engineering these mutations in the other Ace sensors Ace2N-mNeon and VARNAM. The analogous mutations in Ace1m, Mac, and Arch3 also resulted in an inverse polarity in the voltage response, albeit all to different extents.[146]

CONCLUSION

Rhodopsin-based GEVIs have been used as a powerful tool to provide sub-millisecond monitoring of subthreshold neuron dynamics in behaving animals.[131,145,147−149] However, several pitfalls still exist, hindering a wider application in neuroscience. Although the brightness of the single rhodopsin-based sensors has improved a lot, the *in vivo* applications still require high illumination intensity or specialized microscopy, which is not normally offered by commercial microscopes.[131,148] The illumination requirements of rhodopsin eFRET sensors are compatible with conventional microscopes, however the sensitivity is typically low and requirement for synthetic dyes limits applicability for *in vivo* imaging.[141,145,150] However, the major drawback is in the two-photon (2P) imaging performance.[151] While 2P imaging is widely used with GECIs for deep-tissue calcium imaging, successful *in vivo* 2P imaging using rhodopsin-based GEVIs has remained elusive.[152] Although significant improvements have been made on the 2P imaging performance of VSD-based GEVIs, it is still a challenge to use rhodopsin-based GEVIs in 2P imaging.[153,154] Here an improved understanding of the interplay between the structural changes that mutations create, their effect on multiphoton absorption properties, and the dynamics of the photocycle, is crucial. This in turn requires a better understanding of, for instance, the influence of amino acids and water molecules involved in creation of the hydrogen-bond network facilitating the proton transfer process, the states that fluorescence originates from and the effect of voltage on their equilibrium.

By targeting key residues involved in proton transfer, it is possible to adapt the rhodopsin toward desired characteristics.[124,144] Analogous changes can be made to other rhodopsin scaffolds to quickly evaluate their potential as GEVIs and understand the generalizability of design rules. Information on the photocycles from a variety of mutants can lead to optimization of the illumination conditions to accumulate bright and voltage sensitive intermediates for better SNR in 1P and 2P imaging.[132,155]

Single mutations are typically created to positively influence one emergent property of the GEVI protein (brightness, sensitivity, response kinetics, photocurrent) but usually also affect other aspects of GEVI functionality. For example, the counterion is typically the first engineering site to block the proton transfer pathway and eliminate the photocurrent; however mutating the counterion alone often comes at the expense of voltage sensitivity or response kinetics.[156] To optimize GEVI performance, tweaking multiple groups of mutation sites through screening of random mutant libraries is preferable.[127,131,157,158] Recently, *in silico* simulations have demonstrated their complementary ability to decipher the fluorescent and voltage sensitive mechanisms of rhodopsins.[120,159] We anticipate that further developments in machine learning and MD simulations will make it possible to reconstruct a whole time-scale MD simulation model for *in silico* GEVI engineering in the future.

AUTHOR INFORMATION

Corresponding Authors

Daan Brinks − *Department of Imaging Physics, Delft University of Technology, 2628 CJ Delft, The Netherlands; Department of Molecular Genetics, Erasmus University Medical Center, 3015 GD Rotterdam, The Netherlands;* orcid.org/0000-0002-5550-5140; Email: d.brinks@tudelft.nl

Srividya Ganapathy − *Department of Imaging Physics, Delft University of Technology, 2628 CJ Delft, The Netherlands; Department of Pediatrics & Cellular and Molecular Medicine, UCSD School of Medicine, La Jolla, California 92093, United States*; Email: srganapathy@ucsd.edu

Authors

Xin Meng − *Department of Imaging Physics, Delft University of Technology, 2628 CJ Delft, The Netherlands*

Lars van Roemburg − *Department of Imaging Physics, Delft University of Technology, 2628 CJ Delft, The Netherlands*

Marco Post − *Department of Imaging Physics, Delft University of Technology, 2628 CJ Delft, The Netherlands*

Complete contact information is available at: https://pubs.acs.org/10.1021/acsphyschemau.3c00003

Author Contributions

‡X.M. and S.G. contributed equally. The manuscript was written through contributions of all authors. All authors have given approval to the final version of the manuscript. CRediT: **Xin Meng** conceptualization (lead), data curation (lead), formal analysis (lead), investigation (lead), methodology (equal), software (lead), writing-original draft (lead), writing-review & editing (lead); **Srividya Ganapathy** conceptualization (lead), data curation (lead), formal analysis (lead), funding acquisition (supporting), investigation (lead), methodology (lead), writing-original draft (lead), writing-review & editing (lead); **Lars van Roemburg** formal analysis (supporting), investigation (equal), methodology (equal), visualization (equal), writing-review & editing (supporting); **Marco Post** formal analysis (supporting), investigation (equal), methodology (equal), writing-review & editing (supporting); **Daan Brinks** conceptualization (lead), funding acquisition (lead), investigation (supporting), methodology (lead), project administration (lead), resources (lead), supervision (lead), writing-original draft (lead), writing-review & editing (lead).

https://doi.org/10.1021/acsphyschemau.3c00003
ACS Phys. Chem Au XXXX, XXX, XXX−XXX

Funding

D.B. acknowledges support by an NWO Start-up Grant (740.018.018) and ERC Starting Grant (850818-MULTI-VIsion), as well as an NWO XS grant (OCENW.XS2.033). S.G. acknowledges the support of the Human Frontier Science Program Long-term Fellowship (LT000503/2021-L).

Notes

The authors declare no competing financial interest.

■ ACKNOWLEDGMENTS

We gratefully acknowledge Leonie Gouweleeuw, Huma Safar, Mariska Ouwehand, Selina Teurlings, and Didier Duquesnoy for technical support during the research that led to the writing of this review. We thank Marco Locarno, Zhenzhen Wu, Qiangrui Dong, and Rui Silva for valuable discussions.

■ ABBREVIATIONS

BR, Bacteriorhodopsin; RSB, Retinylidene Schiff base; GEVIs, Genetically encoded voltage indicators; GECIs, Genetically encoded calcium indicators; VSDs, Voltage-sensing domains; FPs, Fluorescent proteins; GPR, Bacterial proteorhodopsin; MD, Molecular dynamics; QY, Quantum yield

■ REFERENCES

(1) Kottke, T.; Xie, A.; Larsen, D. S.; Hoff, W. D. Photoreceptors Take Charge: Emerging Principles for Light Sensing. *Annu. Rev. Biophys.* **2018**, *47*, 291−313.
(2) Scheer, H. Biliproteins. *Angew. Chem., Int. Ed. Engl.* **1981**, *20* (3), 241−261.
(3) Ernst, O. P.; Lodowski, D. T.; Elstner, M.; Hegemann, P.; Brown, L. S.; Kandori, H. Microbial and Animal Rhodopsins: Structures, Functions, and Molecular Mechanisms. *Chem. Rev.* **2014**, *114* (1), 126−163.
(4) Spudich, J. L.; Yang, C.-S.; Jung, K.-H.; Spudich, E. N. RETINYLIDENE PROTEINS: Structures and Functions from Archaea to Humans. *Annu. Rev. Cell Dev. Biol.* **2000**, *16*, 365−392.
(5) de Grip, W. J.; Ganapathy, S. Rhodopsins: An Excitingly Versatile Protein Species for Research, Development and Creative Engineering. *Front. Chem.* **2022**, *10*, 879609.
(6) Man, D.; Wang, W.; Sabehi, G.; Aravind, L.; Post, A. F.; Massana, R.; Spudich, E. N.; Spudich, J. L.; Béjà, O. Diversification and Spectral Tuning in Marine Proteorhodopsins. *EMBO J.* **2003**, *22* (8), 1725−1731.
(7) Gómez-Consarnau, L.; Raven, J. A.; Levine, N. M.; Cutter, L. S.; Wang, D.; Seegers, B.; Arístegui, J.; Fuhrman, J. A.; Gasol, J. M.; Sañudo-Wilhelmy, S. A. Microbial Rhodopsins Are Major Contributors to the Solar Energy Captured in the Sea. *Sci. Adv.* **2019**, *5* (8), 8855−8862.
(8) Pushkarev, A.; Inoue, K.; Larom, S.; Flores-Uribe, J.; Singh, M.; Konno, M.; Tomida, S.; Ito, S.; Nakamura, R.; Tsunoda, S. P.; Philosof, A.; Sharon, I.; Yutin, N.; Koonin, E. V.; Kandori, H.; Béjà, O. A Distinct Abundant Group of Microbial Rhodopsins Discovered Using Functional Metagenomics. *Nat.* **2018**, *558* (7711), 595−599.
(9) Boyden, E. S.; Zhang, F.; Bamberg, E.; Nagel, G.; Deisseroth, K. Millisecond-Timescale, Genetically Targeted Optical Control of Neural Activity. *Nat. Neurosci.* **2005**, *8* (9), 1263−1268.
(10) Nagel, G.; Ollig, D.; Fuhrmann, M.; Kateriya, S.; Musti, A. M.; Bamberg, E.; Hegemann, P. Channelrhodopsin-1: A Light-Gated Proton Channel in Green Algae. *Science* **2002**, *296* (5577), 2395−2398.
(11) Kralj, J. M.; Hochbaum, D. R.; Douglass, A. D.; Cohen, A. E. Electrical Spiking in Escherichia Coli Probed with a Fluorescent Voltage-Indicating Protein. *Science* **2011**, *333* (6040), 345−348.
(12) Nakai, J.; Ohkura, M.; Imoto, K. A High Signal-to-Noise Ca2+ Probe Composed of a Single Green Fluorescent Protein. *Nat. Biotechnol.* **2001**, *19* (2), 137−141.
(13) Chen, T. W.; Wardill, T. J.; Sun, Y.; Pulver, S. R.; Renninger, S. L.; Baohan, A.; Schreiter, E. R.; Kerr, R. A.; Orger, M. B.; Jayaraman, V.; Looger, L. L.; Svoboda, K.; Kim, D. S. Ultrasensitive Fluorescent Proteins for Imaging Neuronal Activity. *Nature* **2013**, *499* (7458), 295−300.
(14) Siegel, M. S.; Isacoff, E. Y. A Genetically Encoded Optical Probe of Membrane Voltage. *Neuron* **1997**, *19* (4), 735−741.
(15) Guerrero, G.; Siegel, M. S.; Roska, B.; Loots, E.; Isacoff, E. Y. Tuning FlaSh: Redesign of the Dynamics, Voltage Range, and Color of the Genetically Encoded Optical Sensor of Membrane Potential. *Biophys. J.* **2002**, *83* (6), 3607−3618.
(16) Baker, B. J.; Jin, L.; Han, Z.; Cohen, L. B.; Popovic, M.; Platisa, J.; Pieribone, V. Genetically Encoded Fluorescent Voltage Sensors Using the Voltage-Sensing Domain of Nematostella and Danio Phosphatases Exhibit Fast Kinetics. *J. Neurosci. Methods* **2012**, *208* (2), 190−196.
(17) Yang, H. H. H.; St-Pierre, F.; Sun, X.; Ding, X.; Lin, M. Z. Z.; Clandinin, T. R. R. Subcellular Imaging of Voltage and Calcium Signals Reveals Neural Processing In Vivo. *Cell* **2016**, *166* (1), 245−257.
(18) Kralj, J. M.; Douglass, A. D.; Hochbaum, D. R.; MacLaurin, D.; Cohen, A. E. Optical Recording of Action Potentials in Mammalian Neurons Using a Microbial Rhodopsin. *Nat. Methods* **2012**, *9* (1), 90−95.
(19) Zhang, X. M.; Yokoyama, T.; Sakamoto, M. Imaging Voltage with Microbial Rhodopsins. *Front. Mol. Biosci.* **2021**, *8*, 815.
(20) Chen, D. L.; Wang, G. Y.; Xu, B.; Hu, K. S. All-Trans to 13-Cis Retinal Isomerization in Light-Adapted Bacteriorhodopsin at Acidic PH. *J. Photochem. Photobiol. B Biol.* **2002**, *66* (3), 188−194.
(21) Florean, A. C.; Cardoza, D.; White, J. L.; Lanyi, J. K.; Sension, R. J.; Bucksbaum, P. H. Control of Retinal Isomerization in Bacteriorhodopsin in the High-Intensity Regime. *Proc. Natl. Acad. Sci. U. S. A.* **2009**, *106* (27), 10896−10900.
(22) Gozem, S.; Luk, H. L.; Schapiro, I.; Olivucci, M. Theory and Simulation of the Ultrafast Double-Bond Isomerization of Biological Chromophores. *Chem. Rev.* **2017**, *117* (22), 13502−13565.
(23) Ernst, O. P.; Lodowski, D. T.; Elstner, M.; Hegemann, P.; Brown, L. S.; Kandori, H. Microbial and Animal Rhodopsins: Structures, Functions, and Molecular Mechanisms. *Chem. Rev.* **2014**, *114* (1), 126−163.
(24) Kojima, K.; Kurihara, R.; Sakamoto, M.; Takanashi, T.; Kuramochi, H.; Zhang, X. M.; Bito, H.; Tahara, T.; Sudo, Y. Comparative Studies of the Fluorescence Properties of Microbial Rhodopsins: Spontaneous Emission Versus Photointermediate Fluorescence. *J. Phys. Chem. B* **2020**, *124* (34), 7361−7367.
(25) Lozier, R. H.; Bogomolni, R. A.; Stoeckenius, W. Bacteriorhodopsin: A Light-Driven Proton Pump in Halobacterium Halobium. *Biophys. J.* **1975**, *15* (9), 955.
(26) Govorunova, E. G.; Sineshchekov, O. A.; Li, H.; Spudich, J. L. Microbial Rhodopsins: Diversity, Mechanisms, and Optogenetic Applications. *Annu. Rev. Biochem.* **2017**, *86*, 845−872.
(27) Balashov, S. P.; Ebrey, T. G. Trapping and Spectroscopic Identification of the Photointermediates of Bacteriorhodopsin at Low Temperatures. *Photochem. Photobiol.* **2001**, *73* (5), 453−462.
(28) Lanyi, J. K. Proton Transfers in the Bacteriorhodopsin Photocycle. *Biochim. Biophys. Acta - Bioenerg.* **2006**, *1757* (8), 1012−1018.
(29) Haupts, U.; Tittor, J.; Oesterhelt, D. CLOSING IN ON BACTERIORHODOPSIN: Progress in Understanding the Molecule. *Annu. Rev. Biophys. Biomol. Struct.* **1999**, *28*, 367−399.
(30) Kataoka, M.; Kamikubo, H. Structures of Photointermediates and Their Implications for the Proton Pump Mechanism. *Biochim. Biophys. Acta - Bioenerg.* **2000**, *1460* (1), 166−176.
(31) Zabelskii, D.; Dmitrieva, N.; Volkov, O.; Shevchenko, V.; Kovalev, K.; Balandin, T.; Soloviov, D.; Astashkin, R.; Zinovev, E.; Alekseev, A.; Round, E.; Polovinkin, V.; Chizhov, I.; Rogachev, A.;

https://doi.org/10.1021/acsphyschemau.3c00003
ACS Phys. Chem Au XXXX, XXX, XXX−XXX

Okhrimenko, I.; Borshchevskiy, V.; Chupin, V.; Büldt, G.; Yutin, N.; Bamberg, E.; Koonin, E.; Gordeliy, V. Structure-Based Insights into Evolution of Rhodopsins. *Commun. Biol.* **2021**, *4* (1), 1−12.
(32) Lozier, R. H.; Bogomolni, R. A.; Stoeckenius, W. Bacteriorhodopsin: A Light-Driven Proton Pump in Halobacterium Halobium. *Biophys. J.* **1975**, *15* (9), 955.
(33) Nass Kovacs, G.; Colletier, J. P.; Grünbein, M. L.; Yang, Y.; Stensitzki, T.; Batyuk, A.; Carbajo, S.; Doak, R. B.; Ehrenberg, D.; Foucar, L.; Gasper, R.; Gorel, A.; Hilpert, M.; Kloos, M.; Koglin, J. E.; Reinstein, J.; Roome, C. M.; Schlesinger, R.; Seaberg, M.; Shoeman, R. L.; Stricker, M.; Boutet, S.; Haacke, S.; Heberle, J.; Heyne, K.; Domratcheva, T.; Barends, T. R. M.; Schlichting, I. Three-Dimensional View of Ultrafast Dynamics in Photoexcited Bacteriorhodopsin. *Nat. Commun.* **2019**, *10* (1), 1−17.
(34) Nogly, P.; Weinert, T.; James, D.; Carbajo, S.; Ozerov, D.; Furrer, A.; Gashi, D.; Borin, V.; Skopintsev, P.; Jaeger, K.; Nass, K.; Båth, P.; Bosman, R.; Koglin, J.; Seaberg, M.; Lane, T.; Kekilli, D.; Brünle, S.; Tanaka, T.; Wu, W.; Milne, C.; White, T.; Barty, A.; Weierstall, U.; Panneels, V.; Nango, E.; Iwata, S.; Hunter, M.; Schapiro, I.; Schertler, G.; Neutze, R.; Standfuss, J. Retinal Isomerization in Bacteriorhodopsin Captured by a Femtosecond X-Ray Laser. *Science* **2018**, *361* (6398), eaat0094.
(35) Sharkov, A. V.; Pakulev, A. V.; Chekalin, S. V.; Matveetz, Y. A. Primary Events in Bacteriorhodopsin Probed by Subpicosecond Spectroscopy. *Biochim. Biophys. Acta - Bioenerg.* **1985**, *808* (1), 94−102.
(36) Kobayashi, T.; Saito, T.; Ohtani, H. Real-Time Spectroscopy of Transition States in Bacteriorhodopsin during Retinal Isomerization. *Nat.* **2001**, *414* (6863), 531−534.
(37) Hasson, K. C.; Gai, F.; Anfinrud, P. A. The Photoisomerization of Retinal in Bacteriorhodopsin: Experimental Evidence for a Three-State Model. *Proc. Natl. Acad. Sci. U. S. A.* **1996**, *93* (26), 15124−15129.
(38) Kennis, J. T. M.; Larsen, D. S.; Ohta, K.; Facciotti, M. T.; Glaeser, R. M.; Fleming, G. R. Ultrafast Protein Dynamics of Bacteriorhodopsin Probed by Photon Echo and Transient Absorption Spectroscopy. *J. Phys. Chem. B* **2002**, *106* (23), 6067−6080.
(39) Ye, T.; Gershgoren, E.; Friedman, N.; Ottolenghi, M.; Sheves, M.; Ruhman, S. Resolving the Primary Dynamics of Bacteriorhodopsin, and of a 'C13-C14 Locked' Analog, in the Reactive Excited State. *Chem. Phys. Lett.* **1999**, *314* (5−6), 429−434.
(40) Mathies, R. A.; Brito Cruz, C. H.; Pollard, W. T.; Shank, C. V. Direct Observation of the Femtosecond Excited-State Cis-Trans Isomerization in Bacteriorhodopsin. *Science* **1988**, *240* (4853), 777−779.
(41) Herbst, J.; Heyne, K.; Diller, R. Femtosecond Infrared Spectroscopy of Bacteriorhodopsin Chromophore Isomerization. *Science* **2002**, *297* (5582), 822−825.
(42) Shim, S.; Dasgupta, J.; Mathies, R. A. Femtosecond Time-Resolved Stimulated Raman Reveals the Birth of Bacteriorhodopsin's J and K Intermediates. *J. Am. Chem. Soc.* **2009**, *131* (22), 7592−7597.
(43) Atkinson, G. H.; Ujj, L.; Zhou, Y. Vibrational Spectrum of the J-625 Intermediate in the Room Temperature Bacteriorhodopsin Photocycle. *J. Phys. Chem. A* **2000**, *104* (18), 4130−4139.
(44) Stoeckenius, W.; Lozier, R. H. Light Energy Conversion in Halobacterium Halobium. *J. Supramol. Struct.* **1974**, *2* (5−6), 769−774.
(45) Dobler, J.; Zinth, W.; Kaiser, W.; Oesterhelt, D. Excited-State Reaction Dynamics of Bacteriorhodopsin Studied by Femtosecond Spectroscopy. *Chem. Phys. Lett.* **1988**, *144* (2), 215−220.
(46) Diller, R.; Maiti, S.; Walker, G. C.; Cowen, B. R.; Pippenger, R.; Bogomolni, R. A.; Hochstrasser, R. M. Femtosecond Time-Resolved Infrared Laser Study of the J−K Transition of Bacteriorhodopsin. *Chem. Phys. Lett.* **1995**, *241* (1−2), 109−115.
(47) Brack, T. L.; Atkinson, G. H. Vibrationaily Excited Retinal In the Bacterlorhodopsln Photocycle: Picosecond Time-Resolved Anti-Stokes Resonance Raman Scattering. *J. Phys. Chem.* **1991**, *95*, 2351−2356.
(48) Doig, S. J.; Reid, P. J.; Mathies, R. A. Picosecond Time-Resolved Resonance Raman Spectroscopy of Bacterlorhodopsin's J, K, and KL Intermediates. *J. Am. Chem. Soc.* **1991**, *95*, 6372.
(49) Smith, S. O.; Pardoen, J. A.; Lugtenburg, J.; Mathies, R. A. Vibrational Analysis of the 13-Cis-Retinal Chromophore in Dark-Adapted Bacteriorhodopsin. *J. Phys. Chem.* **1987**, *91* (4), 804−819.
(50) Hage, W.; Kim, M.; Frei, H.; Mathies, R. A. Protein Dynamics in the Bacteriorhodopsin Photocycle: A Nanosecond Step-Scan Ftir Investigation of the KL to L Transition. *J. Phys. Chem.* **1996**, *100* (39), 16026−16033.
(51) Sasaki, J.; Yuzawa, T.; Kandori, H.; Maeda, A.; Hamaguchi, H. Nanosecond Time-Resolved Infrared Spectroscopy Distinguishes Two K Species in the Bacteriorhodopsin Photocycle. *Biophys. J.* **1995**, *68* (5), 2073−2080.
(52) Braiman, M. S.; Mogi, T. M.; Marti, T. M.; Stern, L. J.; Khorana, H. G.; Rothschild, K. J. Vibrational Spectroscopy of Bacteriorhodopsin Mutants: Light-Driven Proton Transport Involves Protonation Changes of Aspartic Acid Residues 85, 96, and 212. *Biochem.* **1988**, *27* (23), 8516−8520.
(53) Druckmann, S.; Ottolenghi, M.; Pande, A.; Pande, J.; Callender, R. H. Acid-Base Equilibrium of the Schiff Base in Bacteriorhodopsin. *Biochemistry* **1982**, *21* (20), 4953−4959.
(54) Chang, C. H.; Chen, J. G.; Govindjee, R.; Ebrey, T. Cation Binding by Bacteriorhodopsin. *Proc. Natl. Acad. Sci. U. S. A.* **1985**, *82* (2), 396−400.
(55) Hendrickson, F. M.; Burkard, F.; Glaeser, R. M. Structural Characterization of the L-to-M Transition of the Bacteriorhodopsin Photocycle. *Biophys. J.* **1998**, *75* (3), 1446−1454.
(56) Kandori, H.; Yamazaki, Y.; Sasaki, J.; Maeda, A.; Needleman, R.; Lanyi, J. K. Water-Mediated Proton Transfer in Proteins: An FTIR Study of Bacteriorhodopsin. *J. Am. Chem. Soc.* **1995**, *117* (7), 2118−2119.
(57) Tanimoto, T.; Furutani, Y.; Kandori, H. Structural Changes of Water in the Schiff Base Region of Bacteriorhodopsin: Proposal of a Hydration Switch Model. *Biochemistry* **2003**, *42* (8), 2300−2306.
(58) Lanyi, J. K.; Schobert, B. Mechanism of Proton Transport in Bacteriorhodopsin from Crystallographic Structures of the K, L, M1, M2, and M2′ Intermediates of the Photocycle. *J. Mol. Biol.* **2003**, *328* (2), 439−450.
(59) Gerwert, K.; Souvignier, G.; Hess, B. Simultaneous Monitoring of Light-Induced Changes in Protein Side-Group Protonation, Chromophore Isomerization, and Backbone Motion of Bacteriorhodopsin by Time-Resolved Fourier-Transform Infrared Spectroscopy. *Proc. Natl. Acad. Sci. U. S. A.* **1990**, *87* (24), 9774−9778.
(60) Braiman, M.; Mathies, R. Resonance Raman Evidence for an All-Trans to 13-Cis Isomerization in the Proton-Pumping Cycle of Bacteriorhodopsin. *Biochemistry* **1980**, *19* (23), 5421−5428.
(61) Gerwert, K.; Siebert, F. Evidence for Light-Induced 13-Cis, 14-s-Cis Isomerization in Bacteriorhodopsin Obtained by FTIR Difference Spectroscopy Using Isotopically Labelled Retinals. *EMBO J.* **1986**, *5* (4), 805−811.
(62) Fodor, S. P. A.; Pollard, W. T.; Gebhard, R.; Van Den Berg, E. M. M.; Lugtenburg, J.; Mathies, R. A. Bacteriorhodopsin's L550 Intermediate Contains a C14-C15 s-Trans-Retinal Chromophore. *Proc. Natl. Acad. Sci. U. S. A.* **1988**, *85* (7), 2156−2160.
(63) Subramaniam, S.; Henderson, R. Molecular Mechanism of Vectorial Proton Translocation by Bacteriorhodopsin. *Nature* **2000**, *406* (6796), 653−657.
(64) Zimányi, L.; Váró, G.; Chang, M.; Ni, B.; Needleman, R.; Lanyi, J. K. Pathways of Proton Release in the Bacteriorhodopsin Photocycle. *Biochemistry* **1992**, *31* (36), 8535−8543.
(65) Herzfeld, J.; Lansing, J. C. Magnetic Resonance Studies of the Bacteriorhodopsin Pump Cycle. *Annu. Rev. Biophys. Biomol. Struct.* **2002**, *31*, 73−95.
(66) Herzfeld, J.; Tounge, B. NMR Probes of Vectoriality in the Proton-Motive Photocycle of Bacteriorhodopsin: Evidence for an 'Electrostatic Steering' Mechanism. *Biochim. Biophys. Acta - Bioenerg.* **2000**, *1460* (1), 95−105.

https://doi.org/10.1021/acsphyschemau.3c00003
ACS Phys. Chem Au XXXX, XXX, XXX−XXX

(67) Subramaniam, S.; Gerstein, M.; Oesterhelt, D.; Henderson, R. Electron Diffraction Analysis of Structural Changes in the Photocycle of Bacteriorhodopsin. *EMBO J.* **1993**, *12* (1), 1−8.
(68) Schobert, B.; Lanyi, J. K. Halorhodopsin Is a Light-Driven Chloride Pump. *J. Biol. Chem.* **1982**, *257* (17), 10306−10313.
(69) Brown, L. S.; Kamikubo, H.; Zimányi, L.; Kataoka, M.; Tokunaga, F.; Verdegem, P.; Lugtenburg, J.; Lanyi, J. K. A Local Electrostatic Change Is the Cause of the Large-Scale Protein Conformation Shift in Bacteriorhodopsin. *Proc. Natl. Acad. Sci. U. S. A.* **1997**, *94* (10), 5040−5044.
(70) Heberle, J. Proton Transfer Reactions across Bacteriorhodopsin and along the Membrane. *Biochim. Biophys. Acta - Bioenerg.* **2000**, *1458* (1), 135−147.
(71) Subramaniam, S.; Faruqi, A. R.; Oesterhelt, D.; Henderson, R. Electron Diffraction Studies of Light-Induced Conformational Changes in the Leu-93 → Ala Bacteriorhodopsin Mutant. *Proc. Natl. Acad. Sci. U. S. A.* **1997**, *94* (5), 1767−1772.
(72) Subramaniam, S.; Henderson, R. Crystallographic Analysis of Protein Conformational Changes in the Bacteriorhodopsin Photocycle. *Biochim. Biophys. Acta - Bioenerg.* **2000**, *1460* (1), 157−165.
(73) Dioumaev, A. K.; Richter, H. T.; Brown, L. S.; Tanio, M.; Tuzi, S.; Saitô, H.; Kimura, Y.; Needleman, R.; Lanyi, J. K. Existence of a Proton Transfer Chain in Bacteriorhodopsin: Participation of Glu-194 in the Release of Protons to the Extracellular Surface. *Biochemistry* **1998**, *37* (8), 2496−2506.
(74) Garczarek, F.; Brown, L. S.; Lanyi, J. K.; Gerwert, K. Proton Binding within a Membrane Protein by a Protonated Water Cluster. *Proc. Natl. Acad. Sci. U. S. A.* **2005**, *102* (10), 3633−3638.
(75) Balashov, S. P.; Imasheva, E. S.; Govindjee, R.; Ebrey, T. G. Titration of Aspartate-85 in Bacteriorhodopsin: What It Says about Chromophore Isomerization and Proton Release. *Biophys. J.* **1996**, *70* (1), 473−481.
(76) Richter, H. T.; Brown, L. S.; Needleman, R.; Lanyi, J. K. A Linkage of the PK(a)'s of Asp-85 and Glu-204 Forms Part of the Reprotonation Switch of Bacteriorhodopsin. *Biochemistry* **1996**, *35* (13), 4054−4062.
(77) Richter, H. T.; Needleman, R.; Lanyi, J. K. Perturbed Interaction between Residues 85 and 204 in Tyr-185−>Phe and Asp-85−>Glu Bacteriorhodopsins. *Biophys. J.* **1996**, *71* (6), 3392−3398.
(78) Sass, H. J.; Büldt, G.; Gessenich, R.; Hehn, D.; Neff, D.; Schlesinger, R.; Berendzen, J.; Ormos, P. Structural Alterations for Proton Translocation in the M State of Wild-Type Bacteriorhodopsin. *Nature* **2000**, *406* (6796), 649−653.
(79) Luecke, H.; Schobert, B.; Cartailler, J. P.; Richter, H. T.; Rosengarth, A.; Needleman, R.; Lanyi, J. K. Coupling Photoisomerization of Retinal to Directional Transport in Bacteriorhodopsin. *J. Mol. Biol.* **2000**, *300* (5), 1237−1255.
(80) Schobert, B.; Brown, L. S.; Lanyi, J. K. Crystallographic Structures of the M and N Intermediates of Bacteriorhodopsin: Assembly of a Hydrogen-Bonded Chain of Water Molecules Between Asp-96 and the Retinal Schiff Base. *J. Mol. Biol.* **2003**, *330* (3), 553−570.
(81) Shibata, M.; Yamashita, H.; Uchihashi, T.; Kandori, H.; Ando, T. High-Speed Atomic Force Microscopy Shows Dynamic Molecular Processes in Photoactivated Bacteriorhodopsin. *Nat. Nanotechnol.* **2010**, *5* (3), 208−212.
(82) Cao, Y.; Lanyi, J. K.; Váró, G.; Chang, M.; Ni, B.; Needleman, R. Water Is Required for Proton Transfer from Aspartate-96 to the Bacteriorhodopsin Schiff Base. *Biochemistry* **1991**, *30* (45), 10972−10979.
(83) Roux, B.; Nina, M.; Pomès, R.; Smith, J. C. Thermodynamic Stability of Water Molecules in the Bacteriorhodopsin Proton Channel: A Molecular Dynamics Free Energy Perturbation Study. *Biophys. J.* **1996**, *71* (2), 670−681.
(84) Otto, H.; Marti, T.; Holz, M.; Mogi, T.; Lindau, M.; Khorana, H. G.; Heyn, M. P. Aspartic Acid-96 Is the Internal Proton Donor in the Reprotonation of the Schiff Base of Bacteriorhodopsin. *Proc. Natl. Acad. Sci. U. S. A.* **1989**, *86* (23), 9228−9232.
(85) Gerwert, K.; Hess, B.; Soppa, J.; Oesterhelt, D. Role of Aspartate-96 in Proton Translocation by Bacteriorhodopsin. *Proc. Natl. Acad. Sci. U. S. A.* **1989**, *86* (13), 4943−4947.
(86) Smith, S. O.; Curry, B.; Mathies, R.; Pardoen, J. A.; Mulder, P. P. J.; Lugtenburg, J. Chromophore Structure in Bacteriorhodopsin's O640 Photointermediate. *Biochemistry* **1983**, *22* (26), 6141−6148.
(87) Dioumaev, A. K.; Brown, L. S.; Needleman, R.; Lanyi, J. K. Partitioning of Free Energy Gain between the Photoisomerized Retinal and the Protein in Bacteriorhodopsin. *Biochemistry* **1998**, *37* (28), 9889−9893.
(88) Brown, L. S.; Needleman, R.; Lanyi, J. K. Functional Roles of Aspartic Acid Residues at the Cytoplasmic Surface of Bacteriorhodopsin. *Biochemistry* **1999**, *38* (21), 6855−6861.
(89) Schätzler, B.; Dencher, N. A.; Tittor, J.; Oesterhelt, D.; Yaniv-Checover, S.; Nachliel, E.; Gutman, M. Subsecond Proton-Hole Propagation in Bacteriorhodopsin. *Biophys. J.* **2003**, *84* (1), 671−686.
(90) Kandt, C.; Schlitter, J.; Gerwert, K. Dynamics of Water Molecules in the Bacteriorhodopsin Trimer in Explicit Lipid/Water Environment. *Biophys. J.* **2004**, *86* (2), 705−717.
(91) Nachliel, E.; Gutman, M.; Tittor, J.; Oesterhelt, D. Proton Transfer Dynamics on the Surface of the Late M State of Bacteriorhodopsin. *Biophys. J.* **2002**, *83* (1), 416−426.
(92) Zscherp, C.; Heberle, J. Infrared Difference Spectra of the Intermediates L, M, N, and O of the Bacteriorhodopsin Photoreaction Obtained by Time-Resolved Attenuated Total Reflection Spectroscopy. *J. Phys. Chem. B* **1997**, *101* (49), 10542−10547.
(93) Gerwert, K.; Freier, E.; Wolf, S. The Role of Protein-Bound Water Molecules in Microbial Rhodopsins. *Biochim. Biophys. Acta - Bioenerg.* **2014**, *1837* (5), 606−613.
(94) Luecke, H.; Richter, H. T.; Lanyi, J. K. Proton Transfer Pathways in Bacteriorhodopsin at 2.3 Angstrom Resolution. *Science* **1998**, *280* (5371), 1934−1937.
(95) Govindjee, R.; Misra, S.; Balashov, S. P.; Ebrey, T. G.; Crouch, R. K.; Menick, D. R. Arginine-82 Regulates the PKa of the Group Responsible for the Light-Driven Proton Release in Bacteriorhodopsin. *Biophys. J.* **1996**, *71* (2), 1011−1023.
(96) Dioumaev, A. K.; Brown, L. S.; Needleman, R.; Lanyi, J. K. Fourier Transform Infrared Spectra of a Late Intermediate of the Bacteriorhodopsin Photocycle Suggest Transient Protonation of Asp-212. *Biochemistry* **1999**, *38* (31), 10070−10078.
(97) Balashov, S. P.; Imasheva, E. S.; Ebrey, T. G.; Chen, N.; Menick, D. R.; Crouch, R. K. Glutamate-194 to Cysteine Mutation Inhibits Fast Light-Induced Proton Release in Bacteriorhodopsin. *Biochemistry* **1997**, *36* (29), 8671−8676.
(98) Dioumaev, A. K.; Richter, H. T.; Brown, L. S.; Tanio, M.; Tuzi, S.; Saitô, H.; Kimura, Y.; Needleman, R.; Lanyi, J. K. Existence of a Proton Transfer Chain in Bacteriorhodopsin: Participation of Glu-194 in the Release of Protons to the Extracellular Surface. *Biochemistry* **1998**, *37* (8), 2496−2506.
(99) Kouyama, T.; Kinosita, K.; Ikegami, A. Excited-State Dynamics of Bacteriorhodopsin. *Biophys. J.* **1985**, *47* (1), 43.
(100) Govindjee, R.; Becher, B.; Ebrey, T. G. The Fluorescence from the Chromophore of the Purple Membrane Protein. *Biophys. J.* **1978**, *22* (1), 67−77.
(101) Marín, M. D. C.; Agathangelou, D.; Orozco-Gonzalez, Y.; Valentini, A.; Kato, Y.; Abe-Yoshizumi, R.; Kandori, H.; Choi, A.; Jung, K. H.; Haacke, S.; Olivucci, M. Fluorescence Enhancement of a Microbial Rhodopsin via Electronic Reprogramming. *J. Am. Chem. Soc.* **2019**, *141* (1), 262−271.
(102) Tittor, J.; Oesterhelt, D. The Quantum Yield of Bacteriorhodopsin. *FEBS Lett.* **1990**, *263* (2), 269−273.
(103) Govindjee, R.; Balashov, S. P.; Ebrey, T. G. Quantum Efficiency of the Photochemical Cycle of Bacteriorhodopsin. *Biophys. J.* **1990**, *58* (3), 597−608.
(104) Ohtani, H.; Tsukamoto, Y.; Sakoda, Y.; Hamaguchi, H. o. Fluorescence Spectra of Bacteriorhodopsin and the Intermediates O and Q at Room Temperature. *FEBS Lett.* **1995**, *359* (1), 65−68.
(105) Ohtani, H.; Kaneko, M.; Ishikawa, M.; Kamiya, N.; Yamamoto, N. Picosecond-Millisecond Dual-Time-Base Spectroscopy

https://doi.org/10.1021/acsphyschemau.3c00003
ACS Phys. Chem Au XXXX, XXX, XXX−XXX

of Fluorescent Photointermediates Formed in the Purple Membrane of Halobacterium Halobium. *Chem. Phys. Lett.* **1999**, *299* (6), 571−575.
(106) Kamiya, N.; Ishikawa, M.; Kasahara, K.; Kaneko, M.; Yamamoto, N.; Ohtani, H. Picosecond Fluorescence Spectroscopy of the Purple Membrane of Halobacterium Halobium in Alkaline Suspension. *Chem. Phys. Lett.* **1997**, *265* (6), 595−599.
(107) Fodor, S. P. A.; Ames, J. B.; Gebhard, R.; Van Den Berg, E. M. M.; Lugtenburg, J.; Mathies, R. A. Chromophore Structure In Bacteriorhodopsin'S N Intermediate: Implications For The Proton-Pumping Mechanism. *Biochemistry* **1988**, *27* (18), 7097−7101.
(108) Nagel, G.; Kelety, B.; Möckel, B.; Büldt, G.; Bamberg, E. Voltage Dependence of Proton Pumping by Bacteriorhodopsin Is Regulated by the Voltage-Sensitive Ratio of M1 to M2. *Biophys. J.* **1998**, *74* (1), 403−412.
(109) Geibel, S.; Friedrich, T.; Ormos, P.; Wood, P. G.; Nagel, G.; Bamberg, E. The Voltage-Dependent Proton Pumping in Bacteriorhodopsin Is Characterized by Optoelectric Behavior. *Biophys. J.* **2001**, *81* (4), 2059−2068.
(110) Karvaly, B.; Dancshazy, Z. Bacteriorhodopsin: A Molecular Photoelectric Regulator Quenching of Photovoltaic Effect of Bimolecular Lipid Membranes Containing Bacteriorhodopsin by Blue Light. *FEBS Lett.* **1977**, *76* (1), 36−40.
(111) Ormos, P.; Dancsházy, Z.; Keszthelyi, L. Electric Response of a Back Photoreaction in the Bacteriorhodopsin Photocycle. *Biophys. J.* **1980**, *31* (2), 207−213.
(112) Tsunoda, S. P.; Ewers, D.; Gazzarrini, S.; Moroni, A.; Gradmann, D.; Hegemann, P. H+-Pumping Rhodopsin from the Marine Alga Acetabularia. *Biophys. J.* **2006**, *91* (4), 1471−1479.
(113) Kawanabe, A.; Furutani, Y.; Jung, K. H.; Kandori, H. Photochromism of Anabaena Sensory Rhodopsin. *J. Am. Chem. Soc.* **2007**, *129* (27), 8644−8649.
(114) Broser, M.; Spreen, A.; Konold, P. E.; Peter, E.; Adam, S.; Borin, V.; Schapiro, I.; Seifert, R.; Kennis, J. T. M.; Bernal Sierra, Y. A.; Hegemann, P. NeoR, a near-Infrared Absorbing Rhodopsin. *Nat. Commun.* **2020**, *11* (1), 1−10.
(115) Song, L.; El-Sayed, M. A.; Lanyi, J. K. Protein Catalysis of the Retinal Subpicosecond Photoisomerization in the Primary Process of Bacteriorhodopsin Photosynthesis. *Science.* **1993**, *261* (5123), 891−894.
(116) Logunov, S. L.; El-Sayed, M. A.; Lanyi, J. K. Catalysis of the Retinal Subpicosecond Photoisomerization Process in Acid Purple Bacteriorhodopsin and Some Bacteriorhodopsin Mutants by Chloride Ions. *Biophys. J.* **1996**, *71* (3), 1545−1553.
(117) Maclaurin, D.; Venkatachalam, V.; Lee, H.; Cohen, A. E. Mechanism of Voltage-Sensitive Fluorescence in a Microbial Rhodopsin. *Proc. Natl. Acad. Sci. U. S. A.* **2013**, *110* (15), 5939−5944.
(118) Saint Clair, E. C.; Ogren, J. I.; Mamaev, S.; Russano, D.; Kralj, J. M.; Rothschild, K. J. Near-IR Resonance Raman Spectroscopy of Archaerhodopsin 3: Effects of Transmembrane Potential. *J. Phys. Chem. B* **2012**, *116* (50), 14592−14601.
(119) Mei, G.; Cavini, C. M.; Mamaeva, N.; Wang, P.; DeGrip, W. J.; Rothschild, K. J. Optical Switching Between Long-Lived States of Opsin Transmembrane Voltage Sensors. *Photochem. Photobiol.* **2021**, *97* (5), 1001−1015.
(120) Silapetere, A.; Hwang, S.; Hontani, Y.; Fernandez Lahore, R. G.; Balke, J.; Escobar, F. V.; Tros, M.; Konold, P. E.; Matis, R.; Croce, R.; Walla, P. J.; Hildebrandt, P.; Alexiev, U.; Kennis, J. T. M.; Sun, H.; Utesch, T.; Hegemann, P. QuasAr Odyssey: The Origin of Fluorescence and Its Voltage Sensitivity in Microbial Rhodopsins. *Nat. Commun.* **2022**, *13* (1), 1−20.
(121) Dioumaev, A. K.; Wang, J. M.; Bálint, Z.; Váró, G.; Lanyi, J. K. Proton Transport by Proteorhodopsin Requires That the Retinal Schiff Base Counterion Asp-97 Be Anionic. *Biochemistry* **2003**, *42* (21), 6582−6587.
(122) Chow, B. Y.; Han, X.; Dobry, A. S.; Qian, X.; Chuong, A. S.; Li, M.; Henninger, M. A.; Belfort, G. M.; Lin, Y.; Monahan, P. E.; Boyden, E. S. High-Performance Genetically Targetable Optical Neural Silencing by Light-Driven Proton Pumps. *Nature* **2010**, *463* (7277), 98−102.
(123) Tittor, J.; Schweiger, U.; Oesterhelt, D.; Bamberg, E. Inversion of Proton Translocation in Bacteriorhodopsin Mutants D85N, D85T, and D85,96N. *Biophys. J.* **1994**, *67* (4), 1682−1690.
(124) Gong, Y.; Li, J. Z.; Schnitzer, M. J. Enhanced Archaerhodopsin Fluorescent Protein Voltage Indicators. *PLoS One* **2013**, *8* (6), e66959.
(125) Flytzanis, N. C.; Bedbrook, C. N.; Chiu, H.; Engqvist, M. K. M.; Xiao, C.; Chan, K. Y.; Sternberg, P. W.; Arnold, F. H.; Gradinaru, V. Archaerhodopsin Variants with Enhanced Voltage-Sensitive Fluorescence in Mammalian and Caenorhabditis Elegans Neurons. *Nat. Commun.* **2014**, *5* (1), 1−9.
(126) Engqvist, M. K. M.; McIsaac, R. S.; Dollinger, P.; Flytzanis, N. C.; Abrams, M.; Schor, S.; Arnold, F. H. Directed Evolution of Gloeobacter Violaceus Rhodopsin Spectral Properties. *J. Mol. Biol.* **2015**, *427* (1), 205−220.
(127) McIsaac, R. S.; Engqvist, M. K. M.; Wannier, T.; Rosenthal, A. Z.; Herwig, L.; Flytzanis, N. C.; Imasheva, E. S.; Lanyi, J. K.; Balashov, S. P.; Gradinaru, V.; Arnold, F. H. Directed Evolution of a Far-Red Fluorescent Rhodopsin. *Proc. Natl. Acad. Sci. U. S. A.* **2014**, *111* (36), 13034−13039.
(128) Hochbaum, D. R.; Zhao, Y.; Farhi, S. L.; Klapoetke, N.; Werley, C. A.; Kapoor, V.; Zou, P.; Kralj, J. M.; MacLaurin, D.; Smedemark-Margulies, N.; Saulnier, J. L.; Boulting, G. L.; Straub, C.; Cho, Y. K.; Melkonian, M.; Wong, G. K. S.; Harrison, D. J.; Murthy, V. N.; Sabatini, B. L.; Boyden, E. S.; Campbell, R. E.; Cohen, A. E. All-Optical Electrophysiology in Mammalian Neurons Using Engineered Microbial Rhodopsins. *Nat. Methods* **2014**, *11* (8), 825−833.
(129) Fan, L. Z.; Nehme, R.; Adam, Y.; Jung, E. S.; Wu, H.; Eggan, K.; Arnold, D. B.; Cohen, A. E. All-Optical Synaptic Electrophysiology Probes Mechanism of Ketamine-Induced Disinhibition. *Nat. Methods* **2018**, *15* (10), 823−831.
(130) Piatkevich, K. D.; Jung, E. E.; Straub, C.; Linghu, C.; Park, D.; Suk, H. J.; Hochbaum, D. R.; Goodwin, D.; Pnevmatikakis, E.; Pak, N.; Kawashima, T.; Yang, C. T.; Rhoades, J. L.; Shemesh, O.; Asano, S.; Yoon, Y. G.; Freifeld, L.; Saulnier, J. L.; Riegler, C.; Engert, F.; Hughes, T.; Drobizhev, M.; Szabo, B.; Ahrens, M. B.; Flavell, S. W.; Sabatini, B. L.; Boyden, E. S. A Robotic Multidimensional Directed Evolution Approach Applied to Fluorescent Voltage Reporters. *Nat. Chem. Biol.* **2018**, *14* (4), 352−360.
(131) Adam, Y.; Kim, J. J.; Lou, S.; Zhao, Y.; Xie, M. E.; Brinks, D.; Wu, H.; Mostajo-Radji, M. A.; Kheifets, S.; Parot, V.; Chettih, S.; Williams, K. J.; Gmeiner, B.; Farhi, S. L.; Madisen, L.; Buchanan, E. K.; Kinsella, I.; Zhou, D.; Paninski, L.; Harvey, C. D.; Zeng, H.; Arlotta, P.; Campbell, R. E.; Cohen, A. E. Voltage Imaging and Optogenetics Reveal Behaviour-Dependent Changes in Hippocampal Dynamics. *Nature* **2019**, *569* (7756), 413−417.
(132) Chien, M. P.; Brinks, D.; Testa-Silva, G.; Tian, H.; Brooks, F. P.; Adam, Y.; Bloxham, W.; Gmeiner, B.; Kheifets, S.; Cohen, A. E. Photoactivated Voltage Imaging in Tissue with an Archaerhodopsin-Derived Reporter. *Sci. Adv.* **2021**, *7* (19), eabe3216.
(133) Piatkevich, K. D.; Bensussen, S.; Tseng, H. an; Shroff, S. N.; Lopez-Huerta, V. G.; Park, D.; Jung, E. E.; Shemesh, O. A.; Straub, C.; Gritton, H. J.; Romano, M. F.; Costa, E.; Sabatini, B. L.; Fu, Z.; Boyden, E. S.; Han, X. Population Imaging of Neural Activity in Awake Behaving Mice. *Nat.* **2019**, *574* (7778), 413−417.
(134) Fan, L. Z.; Kheifets, S.; Böhm, U. L.; Wu, H.; Piatkevich, K. D.; Xie, M. E.; Parot, V.; Ha, Y.; Evans, K. E.; Boyden, E. S.; Takesian, A. E.; Cohen, A. E. All-Optical Electrophysiology Reveals the Role of Lateral Inhibition in Sensory Processing in Cortical Layer 1. *Cell* **2020**, *180* (3), 521−535.e18.
(135) McIsaac, R. S.; Engqvist, M. K.; Wannier, T.; Rosenthal, A. Z.; Herwig, L.; Flytzanis, N. C.; Imasheva, E. S.; Lanyi, J. K.; Balashov, S. P.; Gradinaru, V.; Arnold, F. H. Directed Evolution of a Far-Red Fluorescent Rhodopsin. *Proc. Nat. Acad. Sci.* **2014**, *111* (36), 13034−13039.
(136) Silapetere, A.; Hwang, S.; Hontani, Y.; Fernandez Lahore, R. G.; Balke, J.; Escobar, F. V.; Tros, M.; Konold, P. E.; Matis, R.; Croce,

https://doi.org/10.1021/acsphyschemau.3c00003
ACS Phys. Chem Au XXXX, XXX, XXX−XXX

R.; Walla, P. J.; Hildebrandt, P.; Alexiev, U.; Kennis, J. T. M.; Sun, H.; Utesch, T.; Hegemann, P. QuasAr Odyssey: The Origin of Fluorescence and Its Voltage Sensitivity in Microbial Rhodopsins. *Nat. Commun.* **2022**, *13* (1), 1−20.
(137) Bayraktar, H.; Fields, A. P.; Kralj, J. M.; Spudich, J. L.; Rothschild, K. J.; Cohen, A. E. Ultrasensitive Measurements of Microbial Rhodopsin Photocycles Using Photochromic FRET. *Photochem. Photobiol.* **2012**, *88* (1), 90−97.
(138) Zou, P.; Zhao, Y.; Douglass, A. D.; Hochbaum, D. R.; Brinks, D.; Werley, C. A.; Harrison, D. J.; Campbell, R. E.; Cohen, A. E. Bright and Fast Multicoloured Voltage Reporters via Electrochromic FRET. *Nat. Commun.* **2014**, *5* (1), 1−10.
(139) Gong, Y.; Wagner, M. J.; Li, J. Z.; Schnitzer, M. J. Imaging Neural Spiking in Brain Tissue Using FRET-Opsin Protein Voltage Sensors. *Nat. Commun.* **2014**, *5* (1), 1−11.
(140) Zou, P.; Zhao, Y.; Douglass, A. D.; Hochbaum, D. R.; Brinks, D.; Werley, C. A.; Harrison, D. J.; Campbell, R. E.; Cohen, A. E. Bright and Fast Multicoloured Voltage Reporters via Electrochromic FRET. *Nat. Commun.* **2014**, *5* (1), 1−10.
(141) Gong, Y.; Huang, C.; Li, J. Z.; Grewe, B. F.; Zhang, Y.; Eismann, S.; Schnitzer, M. J. High-Speed Recording of Neural Spikes in Awake Mice and Flies with a Fluorescent Voltage Sensor. *Science* **2015**, *350* (6266), 1361−1366.
(142) Beck, C.; Gong, Y. A High-Speed, Bright, Red Fluorescent Voltage Sensor to Detect Neural Activity. *Sci. Reports* **2019**, *9* (1), 1−12.
(143) Kannan, M.; Vasan, G.; Huang, C.; Haziza, S.; Li, J. Z.; Inan, H.; Schnitzer, M. J.; Pieribone, V. A. Fast, in Vivo Voltage Imaging Using a Red Fluorescent Indicator. *Nat. Methods* **2018**, *15* (12), 1108−1116.
(144) Liu, S.; Lin, C.; Xu, Y.; Luo, H.; Peng, L.; Zeng, X.; Zheng, H.; Chen, P. R.; Zou, P. A Far-Red Hybrid Voltage Indicator Enabled by Bioorthogonal Engineering of Rhodopsin on Live Neurons. *Nat. Chem.* **2021**, *13* (5), 472−479.
(145) Abdelfattah, A. S.; Kawashima, T.; Singh, A.; Novak, O.; Liu, H.; Shuai, Y.; Huang, Y. C.; Campagnola, L.; Seeman, S. C.; Yu, J.; Zheng, J.; Grimm, J. B.; Patel, R.; Friedrich, J.; Mensh, B. D.; Paninski, L.; Macklin, J. J.; Murphy, G. J.; Podgorski, K.; Lin, B. J.; Chen, T. W.; Turner, G. C.; Liu, Z.; Koyama, M.; Svoboda, K.; Ahrens, M. B.; Lavis, L. D.; Schreiter, E. R. Bright and Photostable Chemigenetic Indicators for Extended in Vivo Voltage Imaging. *Science* **2019**, *365* (6454), 699−704.
(146) Abdelfattah, A. S.; Valenti, R.; Zheng, J.; Wong, A.; Chuong, A. S.; Hasseman, J. P.; Jayaraman, V.; Kolb, I.; Korff, W.; Lavis, L. D.; Liang, Y.; Looger, L. L.; Merryweather, D.; Reep, D.; Spruston, N.; Svoboda, K.; Tsang, A.; Tsegaye, G.; Turner, G.; Podgorski, K.; Koyama, M.; Kim, D. S.; Schreiter, E. R. A General Approach to Engineer Positive-Going EFRET Voltage Indicators. *Nat. Commun.* **2020**, *11* (1), 1−8.
(147) Piatkevich, K. D.; Bensussen, S.; Tseng, H. an; Shroff, S. N.; Lopez-Huerta, V. G.; Park, D.; Jung, E. E.; Shemesh, O. A.; Straub, C.; Gritton, H. J.; Romano, M. F.; Costa, E.; Sabatini, B. L.; Fu, Z.; Boyden, E. S.; Han, X. Population Imaging of Neural Activity in Awake Behaving Mice. *Nature* **2019**, *574* (7778), 413−417.
(148) Fan, L. Z.; Kheifets, S.; Böhm, U. L.; Wu, H.; Piatkevich, K. D.; Xie, M. E.; Parot, V.; Ha, Y.; Evans, K. E.; Boyden, E. S.; Takesian, A. E.; Cohen, A. E. All-Optical Electrophysiology Reveals the Role of Lateral Inhibition in Sensory Processing in Cortical Layer 1. *Cell* **2020**, *180* (3), 521−535.e18.
(149) Gong, Y.; Huang, C.; Li, J. Z.; Grewe, B. F.; Zhang, Y.; Eismann, S.; Schnitzer, M. J. High-Speed Recording of Neural Spikes in Awake Mice and Flies with a Fluorescent Voltage Sensor. *Science* **2015**, *350* (6266), 1361−1366.
(150) Abdelfattah, A. S.; Zheng, J.; Reep, D.; Tsegaye, G.; Tsang, A.; Arthur, B. J.; Rehorova, M.; Olson, C. V.; Huang, Y.-C.; Shuai, Y.; Koyama, M.; Moya, M. V.; Weber, T. D.; Lemire, A. L.; Baker, C. A.; Falco, N.; Zheng, Q.; Grimm, J. B.; Yip, M. C.; Walpita, D.; Forest, C. R.; Chase, M.; Campagnola, L.; Murphy, G.; Wong, A. M.; Mertz, J.; Economo, M. N.; Turner, G.; Lin, B.-J.; Chen, T.-W.; Novak, O.; Lavis, L. D.; Svoboda, K.; Korff, W.; Schreiter, E. R.; Hasseman, J. P.; Kolb, I. Sensitivity Optimization of a Rhodopsin-Based Fluorescent Voltage Indicator. *bioRxiv*, November 11, 2021. DOI: 10.1101/2021.11.09.467909 (accessed 2023-04-06).
(151) Brinks, D.; Klein, A. J.; Cohen, A. E. Two-Photon Lifetime Imaging of Voltage Indicating Proteins as a Probe of Absolute Membrane Voltage. *Biophys. J.* **2015**, *109* (5), 914−921.
(152) Mohr, M. A.; Bushey, D.; Aggarwal, A.; Marvin, J. S.; Kim, J. J.; Marquez, E. J.; Liang, Y.; Patel, R.; Macklin, J. J.; Lee, C. Y.; Tsang, A.; Tsegaye, G.; Ahrens, A. M.; Chen, J. L.; Kim, D. S.; Wong, A. M.; Looger, L. L.; Schreiter, E. R.; Podgorski, K. JYCaMP: An Optimized Calcium Indicator for Two-Photon Imaging at Fiber Laser Wavelengths. *Nat. Methods* **2020**, *17* (7), 694−697.
(153) Liu, Z.; Lu, X.; Villette, V.; Gou, Y.; Colbert, K. L.; Lai, S.; Guan, S.; Land, M. A.; Lee, J.; Assefa, T.; Zollinger, D. R.; Korympidou, M. M.; Vlasits, A. L.; Pang, M. M.; Su, S.; Cai, C.; Froudarakis, E.; Zhou, N.; Patel, S. S.; Smith, C. L.; Ayon, A.; Bizouard, P.; Bradley, J.; Franke, K.; Clandinin, T. R.; Giovannucci, A.; Tolias, A. S.; Reimer, J.; Dieudonné, S.; St-Pierre, F. Sustained Deep-Tissue Voltage Recording Using a Fast Indicator Evolved for Two-Photon Microscopy. *Cell* **2022**, *185* (18), 3408−3425.e29.
(154) Brinks, D.; Klein, A. J.; Cohen, A. E. Two-Photon Lifetime Imaging of Voltage Indicating Proteins as a Probe of Absolute Membrane Voltage. *Biophys. J.* **2015**, *109* (5), 914−921.
(155) Penzkofer, A.; Silapetere, A.; Hegemann, P. Photocycle Dynamics of the Archaerhodopsin 3 Based Fluorescent Voltage Sensor Archon2. *J. Photochem. Photobiol. B Biol.* **2021**, *225*, 112331.
(156) Kralj, J. M.; Douglass, A. D.; Hochbaum, D. R.; MacLaurin, D.; Cohen, A. E. Optical Recording of Action Potentials in Mammalian Neurons Using a Microbial Rhodopsin. *Nat. Methods* **2012**, *9* (1), 90−95.
(157) Piatkevich, K. D.; Jung, E. E.; Straub, C.; Linghu, C.; Park, D.; Suk, H. J.; Hochbaum, D. R.; Goodwin, D.; Pnevmatikakis, E.; Pak, N.; Kawashima, T.; Yang, C. T.; Rhoades, J. L.; Shemesh, O.; Asano, S.; Yoon, Y. G.; Freifeld, L.; Saulnier, J. L.; Riegler, C.; Engert, F.; Hughes, T.; Drobizhev, M.; Szabo, B.; Ahrens, M. B.; Flavell, S. W.; Sabatini, B. L.; Boyden, E. S. A Robotic Multidimensional Directed Evolution Approach Applied to Fluorescent Voltage Reporters. *Nat. Chem. Biol.* **2018**, *14* (4), 352−360.
(158) Hochbaum, D. R.; Zhao, Y.; Farhi, S. L.; Klapoetke, N.; Werley, C. A.; Kapoor, V.; Zou, P.; Kralj, J. M.; MacLaurin, D.; Smedemark-Margulies, N.; Saulnier, J. L.; Boulting, G. L.; Straub, C.; Cho, Y. K.; Melkonian, M.; Wong, G. K. S.; Harrison, D. J.; Murthy, V. N.; Sabatini, B. L.; Boyden, E. S.; Campbell, R. E.; Cohen, A. E. All-Optical Electrophysiology in Mammalian Neurons Using Engineered Microbial Rhodopsins. *Nat. Methods* **2014**, *11* (8), 825−833.
(159) Palombo, R.; Barneschi, L.; Pedraza-González, L.; Padula, D.; Schapiro, I.; Olivucci, M. Retinal Chromophore Charge Delocalization and Confinement Explain the Extreme Photophysics of Neorhodopsin. *Nat. Commun.* **2022**, *13* (1), 1−9.

https://doi.org/10.1021/acsphyschemau.3c00003
ACS Phys. Chem Au XXXX, XXX, XXX−XXX